ARMY RESEARCH LABORATORY

Deformation of a Low-Cost Ti-6A1-4V Armor Alloy Under Shock Loading

by Stephen V. Spletzer and Dattatraya P. Dandekar

ARL-TR-2386 February 2001

The findings in this report are not to be construed as an official Department of the Army position unless so designated by other authorized documents.

Citation of manufacturer's or trade names does not constitute an official endorsement or approval of the use thereof.

Destroy this report when it is no longer needed. Do not return it to the originator.

Army Research Laboratory
Aberdeen Proving Ground, MD 21005-5066

ARL-TR-2386 **February 2001**

Deformation of a Low-Cost Ti-6A1-4V Armor Alloy Under Shock Loading

Stephen V. Spletzer and Dattatraya P. Dandekar
Weapons and Materials Research Directorate, ARL

Abstract

The shock behavior of a new, low-cost Ti-6Al-4V alloy has been characterized up to stress levels of 20 GPa. Examination of the particle velocity histories obtained from specimens of the alloy during 11 plate-on-plate impact/planar shock wave experiments indicates that the alloy deforms in an elastic-plastic manner. The magnitude of the Hugoniot Elastic Limit (HEL) lies between 2.0 and 3.0 GPa and appears to be dependent upon material thickness. Plastic shock velocity increases with increasing stress and varies from 5.20 to 5.53 mm/μs. Reshock experiments indicate material work hardening. Shear strength sustained during plastic deformation also tends to increase with stress and ranges from 0.5 to 0.9 GPa. Spall strength thresholds tend to vary with changes in pulse width and ranges from 3.1 to 4.2 GPa.

Acknowledgments

Dr. B. Roopchand provided seed money and material for the investigation. The authors thank Cliff Hubbard and Jack Mullin for their assistance in obtaining the micrographs presented in this report. Mike Staker is also acknowledged for his assistance in examining the shear deformation of Ti-6Al-4V specimens. The authors also thank Dale Ashwell for his assistance in the assembly of the experiments.

INTENTIONALLY LEFT BLANK.

Table of Contents

INTENTIONALLY LEFT BLANK.

List of Figures

List of Tables

INTENTIONALLY LEFT BLANK.

1. Introduction

Ti-6Al-4V alloy has been used extensively in aircraft and aerospace applications; however, to successfully transition it to widespread use in the military theater as armor for combat vehicles, the production and fabrication costs of this alloy must be reduced. Efforts to meet this goal have resulted in a new Ti-6Al-4V alloy. The material used in the present work was produced from a mix of 32% titanium sponge and 62% Ti-6Al-4V turnings, with the balance made up of aluminum shot and V-Al Master alloy (Burkins et al., to be published). The primary cost savings come from the use of titanium sponge and Ti-6Al-4V turnings. The ingot was electron-beam melted in a cold, water-cooled copper, hearth furnace. The motivation for the present work was to compare the shock response of the low-cost alloy to the alloy of similar composition used in aircraft/aerospace applications. Plate-on-plate impact experiments were performed to obtain information pertaining to the shock, release, re-shock, and tensile behavior of this alloy.

2. Material

The nominal composition of the alloy (in weight-percent) is Al (6.28), V (4.16), O (0.176), Fe (0.151), C (0.025), and N (0.008). The remainder is titanium. The 6.35-cm-thick plate used in this work was annealed at 1,213 K for 2 hr, roller leveled, then annealed at 1,033 K for 1 hr. The microstructure consists of equiaxed alpha phase with intergranular beta phase (Figure 1). The static mechanical properties (yield strength, tensile strength, and ductility measured by elongation and reduction in area under tension) indicated that the material is isotropic (Burkins et al., to be published). Burkins et al. reported the values of yield and tensile strength as 896 ± 13 and 958 ± 7 MPa, respectively. The values of elongation and reduction in area are 13% and 24.5%, respectively. The measured value of density of the alloy is 4.415 ± 0.008 g/cm^3. The measured values of ultrasonic longitudinal and shear wave velocities are 6.12 ± 0.07 and 3.17 ± 0.13 km/s, respectively. These represent averages of density and wave velocity measurements carried out on 21 specimens of the alloy. Differences in the values of density and elastic wave

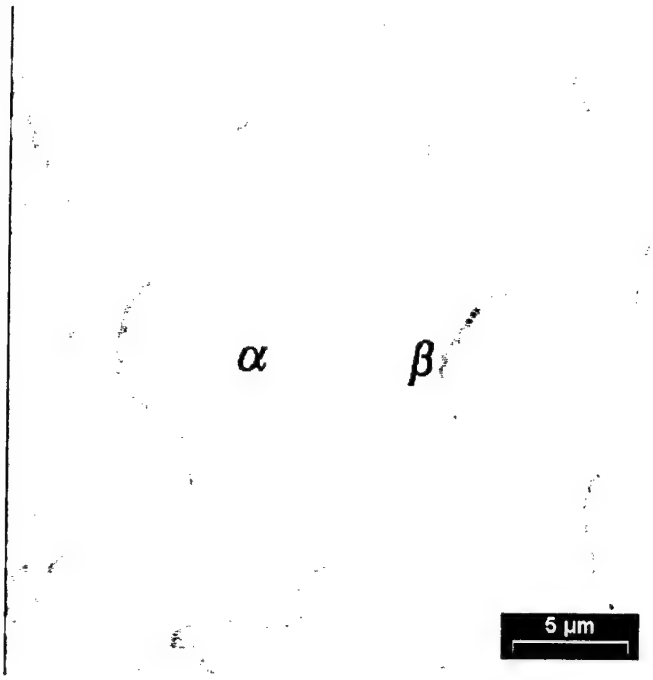

Figure 1. Ti-6Al-4V Microstructure.

velocities of the traditional Ti-6Al-4V alloy and the low-cost alloy used in this work are within the error of the measurements.

3. Test Procedures and Techniques

Ti-6Al-4V specimens used during the shock wave experiments were 40 mm in diameter, with thicknesses of 2–8 mm. Z-cut sapphire and tungsten carbide discs of various thicknesses and diameters were also used as impactors and targets to produce higher stress levels. Initial selection of the specimen thickness was critical to ensuring that data obtained on the shock, release, re-shock, and tensile behavior of the alloy was captured during a state of uniaxial strain. Specimens used in these experiments were lapped until they were flat and parallel within 10 µm. Precise thickness measurements were then taken to the nearest micrometer. Once these preparations were completed, density and ultrasonic sound speed measurements were performed. These measurements are discussed in section 3.1.

Target samples were then prepared to produce a diffuse reflective surface, for use with the laser and velocity interferometry (VISAR) techniques. Using a diffuse reflective surface minimizes the chances of a data signal being lost due to slight misalignments that may occur during the shock wave experiments. Ti-6Al-4V and tungsten carbide samples were hand polished using a diamond paste to produce the desired reflectivity. Sapphire targets were coated with a layer of aluminum in a vacuum evaporator to produce a diffuse reflective surface.

Figure 2 shows the arrangement of the experimental components. Samples were mounted in the appropriate flyer and target ring assemblies with epoxy. The flyer ring assemblies (item no. 1 in Figure 2) were designed to ensure that the impactor successfully reached the target material and produced a normal impact. Once the flyer ring was fully assembled, it was mounted onto an aluminum projectile (item no. 2) and laser aligned to the target to minimize tilt. Tilt levels of these experiments were less than 0.5 mrad. Targets (item no. 3) were assembled with an embedded circuit that was used to detect impact. This open circuit was closed by contact with the flyer ring upon impact. Shorting of this circuit triggered the recording of data via digital oscilloscopes.

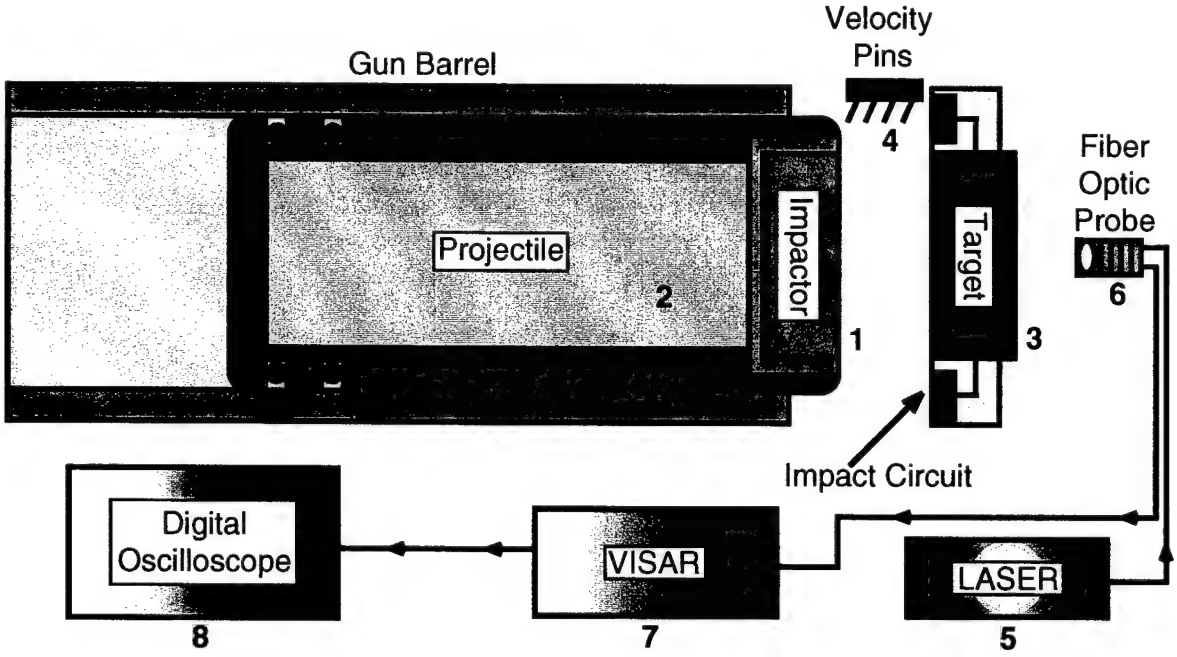

Figure 2. Schematic of a Plate-on-Plate Impact Experiment.

Experiments were performed using a 103-mm-diameter single-stage light gas gun, located at the Gas Gun Facility of the U.S. Army Research Laboratory (ARL) at Aberdeen Proving Ground, MD. Measured projectile velocities ranged from 252–662 m/s, with an uncertainty of less than 0.5%. Velocities were measured by shorting four sets of charged pins (item no. 4), separated by known distances.

Particle velocity profiles were acquired using a Push-Pull VISAR (Hemsing 1979) (item no. 7), and recorded on high-speed digital oscilloscopes (item no. 8). A fiber-optic probe (item no. 6) was mounted 30 mm behind the target. The purpose of the probe was to deliver the beam to the target's center and capture the reflected signal. The laser (item no. 5) used during these experiments was a Class IV Argon-Ion laser. When impact occurred, the probe transmitted a shock-induced velocity history of the target's rear surface to the VISAR. The precision of the VISAR measurements was 1%.

Four types of plate-on-plate impact experimental configurations were prepared to characterize the shock-induced response of the low-cost Ti-6Al-4V alloy. A description of each type can be found in sections 3.2–3.5.

3.1 Density and Ultrasonic Measurements. Density, longitudinal wave velocity, and shear wave velocity are three properties that can be used to calculate the elastic constants of a material. These properties are also useful in the design of plate-on-plate impact experiments, as they can be used to determine the elastic behavior of a material. The elastic wave velocities of a material are obtained from the ultrasonically measured longitudinal and shear wave velocities. The initial density is also used to calculate the material's elastic impedance.

Density measurements were performed on a Sartorius Micro Balance. This system utilizes Archimedes' Principle, taking weight measurements of a sample in both air and water to determine the density. Corrections were made by the system for temperature, air buoyancy, and water adhesion. The accuracy of the system is rated at 0.000070 g.

Ultrasonic sound speed measurements were performed using Matec's MBS-8000 ultrasonic system with their DSP-8000 software. Sound speed measurements were performed by this system utilizing a Pulse-Echo Overlap technique (Papadakis 1967) at a frequency of 5 MHz. This system uses a transducer to send a sound wave into a specimen. A couplant is used between the transducer and specimen to enhance transmission of the sound wave into the material. Two successive pulse echoes from the rear surface of the material are captured by the transducer and overlapped in time. This allows the time between return pulses to be accurately measured. Using the thickness of the sample, the sound speed can be easily determined. A sample wave train, as captured by a 5 MHz transducer, is shown in Figure 3. The first pulse (1) is the input signal from the transducer. The next two pulses (2 and 3) are echoes returning from the rear surface of the Ti-6Al-4V specimen.

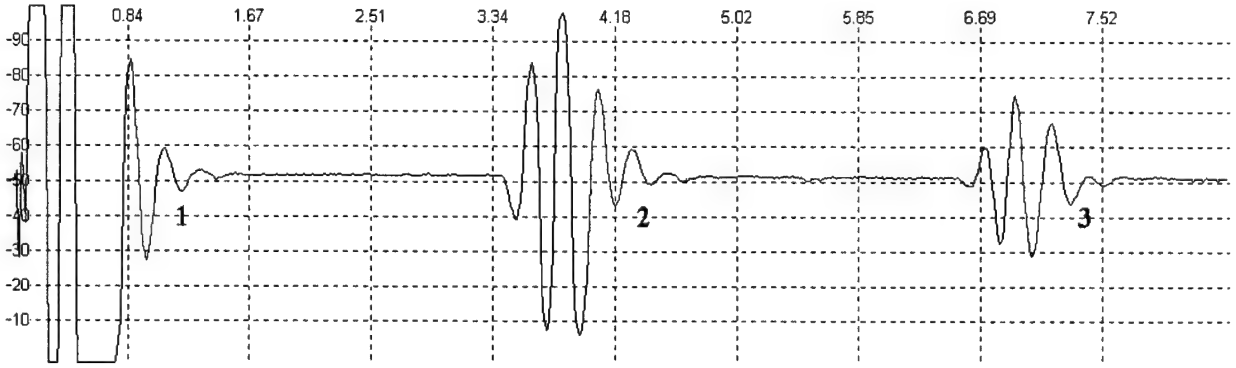

Figure 3. Ultrasonic Wave Train From a Ti-6Al-4V Specimen.

Longitudinal sound speed measurements were performed using a water gap as the couplant. When the transducer is mounted directly to the specimen, reverberations caused by the couplant impart a small phase shift into the return echoes. This decreases the accuracy of the measurements. When a water gap is used as the couplant, the return echoes from the specimen can be spaced apart in time from the reverberations caused by the water-specimen interface. The accuracy of measurements performed in this manner was 0.25%.

Shear sound speed measurements used honey as the couplant. Although the water gap method is more accurate, it cannot be used for shear measurements since water will not support a shear wave. The accuracy of the shear sound speed measurements was 0.50%.

3.2 Transmission Experiments. The purpose of this experiment type is to monitor shock behavior directly from the material of interest. A sample configuration of a transmission experiment is shown in Figure 4. In this configuration, the target is the material to be characterized. A velocity profile obtained via VISAR probe from the target's rear surface provides information on the shock response of the material.

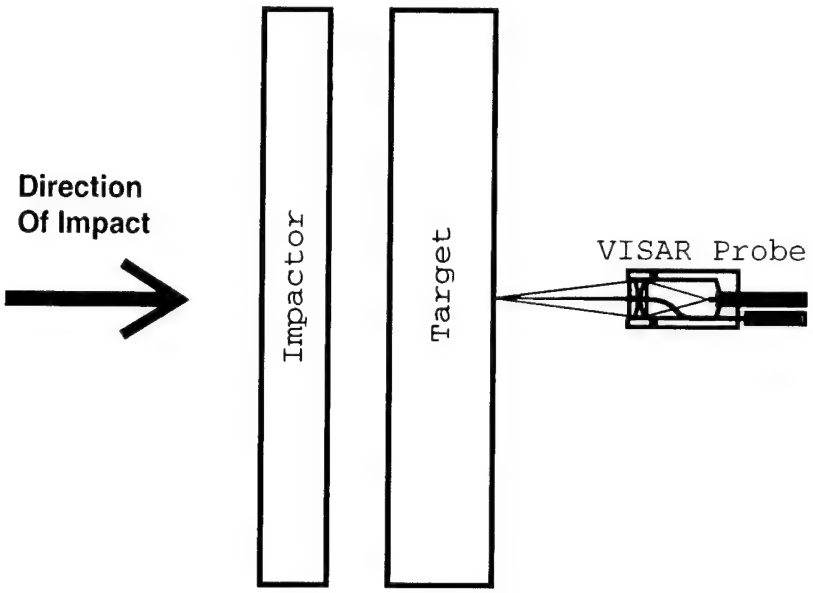

Figure 4. Transmission Experiment Configuration.

To successfully plan a plate-on-plate impact experiment, x-t and a σ-u diagrams need to be developed. These diagrams provide a visual representation of the states materials undergo during plate-on-plate impact experiments. The x-t diagram shows the wave interactions in time, allowing one to predict where and when a stress state or event will occur in a material. Material sound speeds are used in conjunction with specimen thickness to plot out the wave interactions. The σ-u diagram shows the predicted stress states reached by the impactors and targets, using material impedance lines. Material impedance is a function of both the density and sound speed of a material. Stress levels reached by a material depend upon the material impedances and velocity changes.

Figures 5 and 6 are representative x-t and σ-u diagrams for the transmission experiments performed in this work. For ease of identification, the x-t and σ-u diagrams show two different materials. The behavior of the material of interest is mapped out using solid lines, while that of the impactor is shown with dashed lines. However, symmetric impact experiments, where the impactor and target were both Ti-6Al-4V, were also performed. Furthermore, the sample σ-u diagram uses a higher impedance impactor, assumes linear impedance behavior, and equivalent shock and release behavior. Lastly, material thicknesses used in the transmission experiments were selected so that the tensile behavior of the new alloy could also be observed.

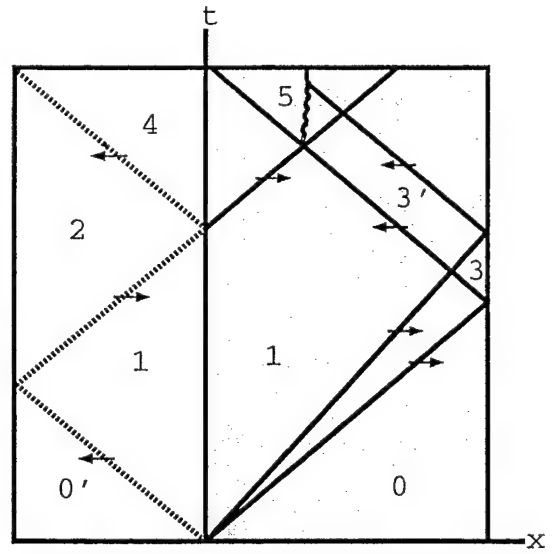

Figure 5. x-t Diagram (Transmission).

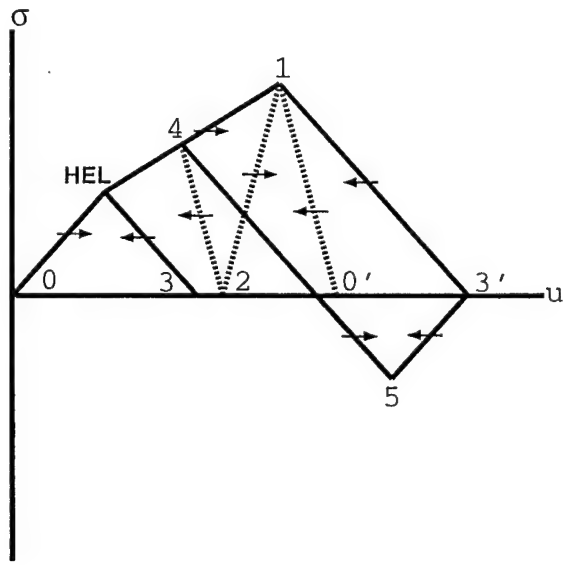

Figure 6. σ-u Diagram (Transmission).

A simplified description of the events occurring in the target and impactor follows. In Figures 5 and 6, prior to impact, the target is at a state of rest (zero stress and particle velocity) while the impactor, which is also at zero stress, moves with the projectile velocity. These initial states are denoted by 0 (target) and 0′ (impactor). Upon impact, both materials shock up to a common state (1). As shown in the x-t diagram, the deformation of the Ti-6Al-4V alloy is attained through the propagation of two shock waves. An elastic wave followed by a slower plastic wave. This is again shown in the σ-u diagram by the two different impedance lines that occur between states 0 and 1, with the Hugoniot Elastic Limit (HEL) as the transition point. The impactor then releases to zero stress at state 2 as the shock wave reaches the free surface. The

shock waves moving in the target also release as they reach a free surface. The first release is caused by the elastic wave releasing to state 3. This corresponds to the elastic region of the velocity profile in Figure 7. This is followed by the release of the plastic wave to a zero stress level at state 3′. The release wave in the impactor reaches the target interface, causing both materials to reach the common state of 4. Interaction of the release waves in the target cause a state of tension, as shown by state 5. If the material fails to support the tension, the material will separate (spall), and a new free surface will be formed at the location of the tension in the target.

Once the x-t and σ-u diagrams have been completed, a representative velocity profile can be created. Since a free surface cannot support a stress, all velocity changes observed by the probe should occur at the zero stress level as shown in the σ-u diagram. From Figure 6, two velocity jumps caused by the release of the elastic and plastic waves to zero stress at states 3 and 3′ were expected. These are shown in Figure 7 as the elastic and plastic regions. Additionally, a sample spall signal is shown. The formation of a spall plane causes the large downward spike to occur in the velocity profile, as the release from state 5 reaches the free surface. This spike is known as the pull-back velocity. If the material does not spall, a sustained velocity decrease will occur as the release wave reaches the free surface.

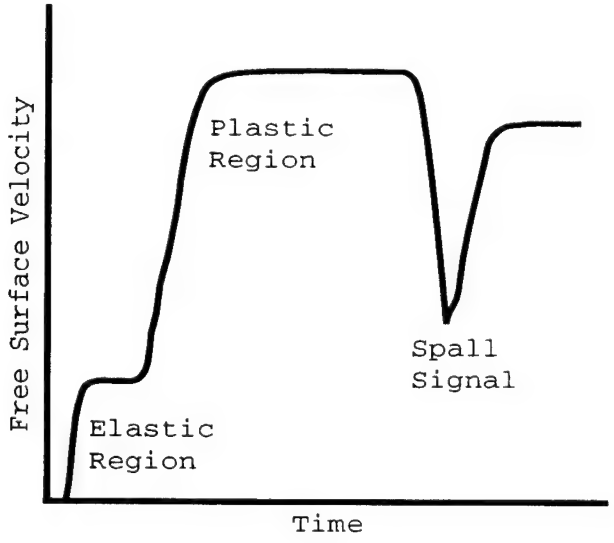

Figure 7. Velocity Profile (Transmission).

3.3 Direct Impact Experiments. This type of experiment is performed to characterize both the initial shock and release behavior of a material (Lysne et al. 1969). The material of interest is used as the impactor and it impacts (preferably) a higher impedance linear elastic target material (Figure 8). The target is typically thin, which allows numerous release reverberations to be recorded during a state of uniaxial strain. These reverberations are used to determine the impactor's behavior.

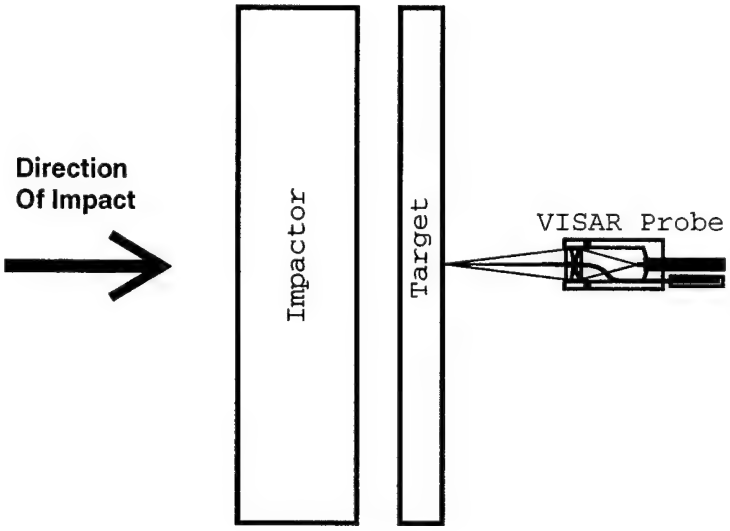

Figure 8. Direct Impact Experiment Configuration.

Figures 9 and 10 show the wave interactions in the x-t and σ-u diagrams. The impactor is thick so that release waves from its free surface do not affect reverberations in the target. The σ-u diagram shows the response of the reverberations (dashed lines) as they bounce off the impactor (solid lines) and release at the free surface. These interactions map out the impactor's initial shock response and release behavior.

The initial states of the target and impactor are denoted as 0 and 0′, respectively. Upon impact, a common state is reached (1). Successive releases at the targets-free surface produce states 2 and 4, which are observed changes in the free surface velocity profile. These changes are used to determine states like 3 and 5, which are reached at the impactor/target interface. For

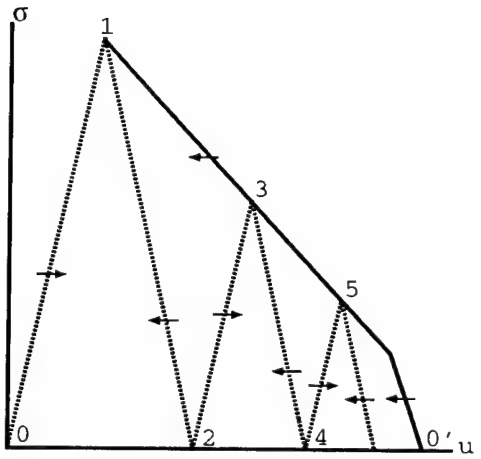

Figure 9. x-t Diagram (Direct Impact).

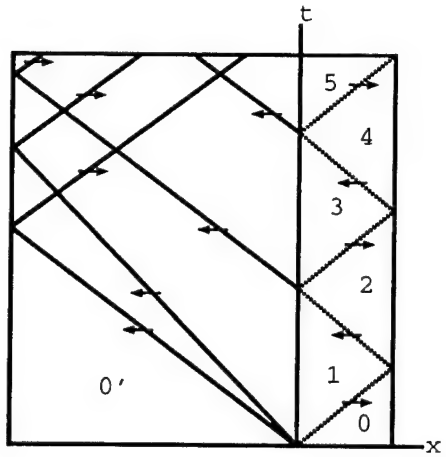

Figure 10. σ-u Diagram (Direct Impact).

simplicity, the shock and release behaviors of the target are identical in the σ-u diagram. Many materials, however, exhibit different shock and release behaviors.

Figure 11 shows a generic velocity profile. The first two velocity jumps correspond to states 2 and 4. The velocity of the target will continue to increase towards the initial impactor velocity, with successive reverberations.

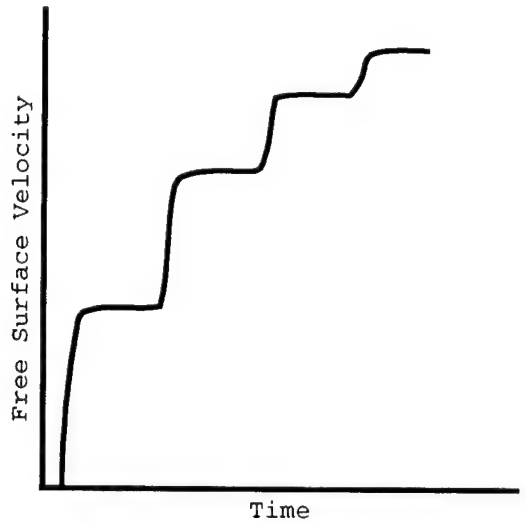

Figure 11. Velocity Profile (Direct Impact).

3.4 Re-Shock Experiments. The re-shock experiment (Asay et al. 1980) uses a two-material target, as shown in the sample configuration of Figure 12. A second higher impedance-target is mounted against the rear of the primary target material. Interactions between the two targets cause re-shocks in the material of interest. This enables shock Hugoniot data to be gathered at higher stress levels. As in the direct impact experiments, the impactor thickness was selected so that return waves from the impactor's free surface did not affect the recorded velocity profile.

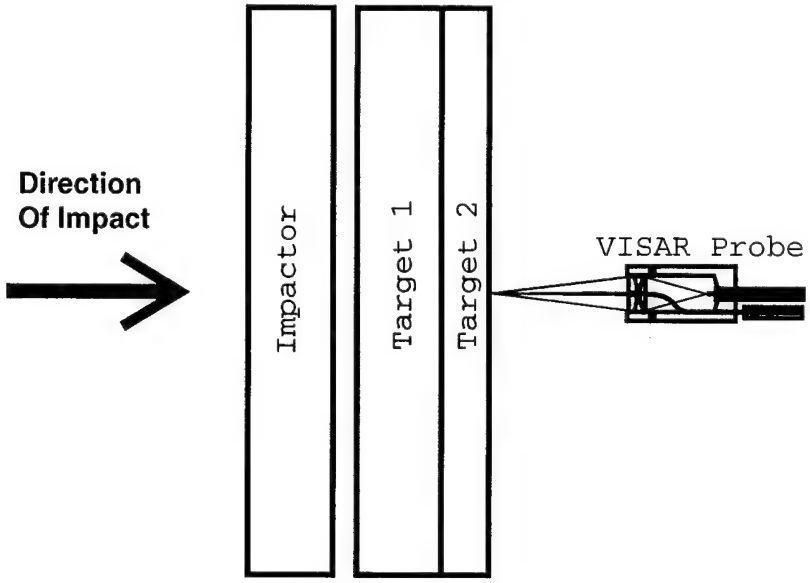

Figure 12. Re-Shock Experiment Configuration.

The x-t and σ-u diagrams (Figures 13 and 14) illustrate the re-shock of target 1. Initial states of the targets and impactors are 0 and 0′, respectively. Impact creates state 1 in the impactor and target 1. Elastic and plastic waves traverse target 1 and interact with target 2. The elastic wave generates state 2 and reflects back into target 1. This shock meets the plastic wave, generating state 3. The plastic wave reaches the target 1/target 2 interface creating the re-shock at state 4. States 5 and 7 occur when waves from the target 1/target 2 interface reach the free surface.

The velocity profile shown in Figure 15 is similar to that of the direct impact experiment. However, the observed velocity increases are not successively smaller. This is due to

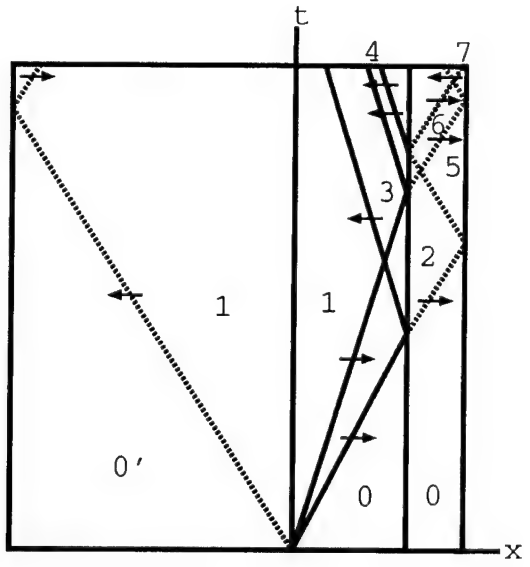

Figure 13. x-t Diagram (Re-Shock).

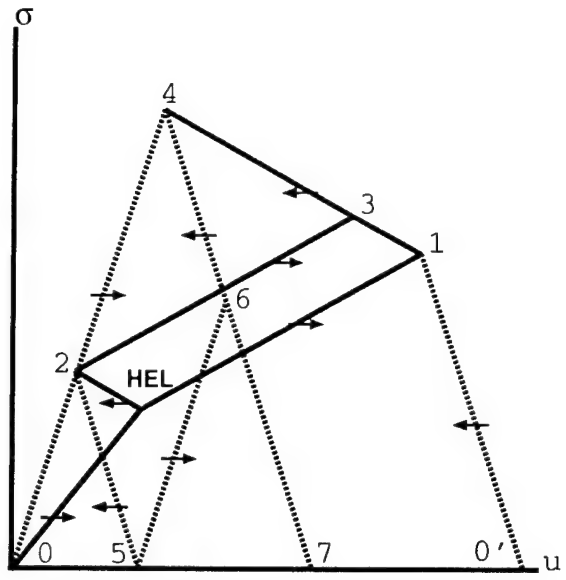

Figure 14. σ-u Diagram (Re-Shock).

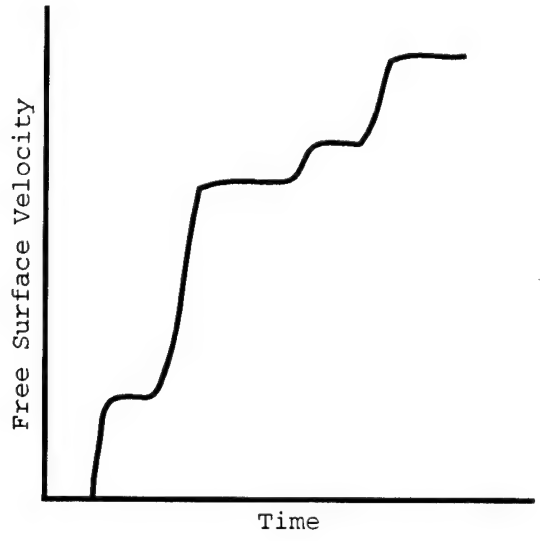

Figure 15. Velocity Profile (Re-Shock).

reverberations from both the elastic and plastic waves in the primary target. The first two velocity jumps would correspond to states 5 and 7 of the x-t and σ-u diagrams.

3.5 Oblique Impact Experiments. The oblique impact is similar to the transmission experiment. However, in this case, the impactor and target are mounted at an angle (Figure 16), with a VISAR probe mounted normal to the target's rear surface. Upon impact both longitudinal and shear waves propagate through the materials, increasing the level of shear deformation from what is normally seen in a transmission experiment, as described in section 3.2.

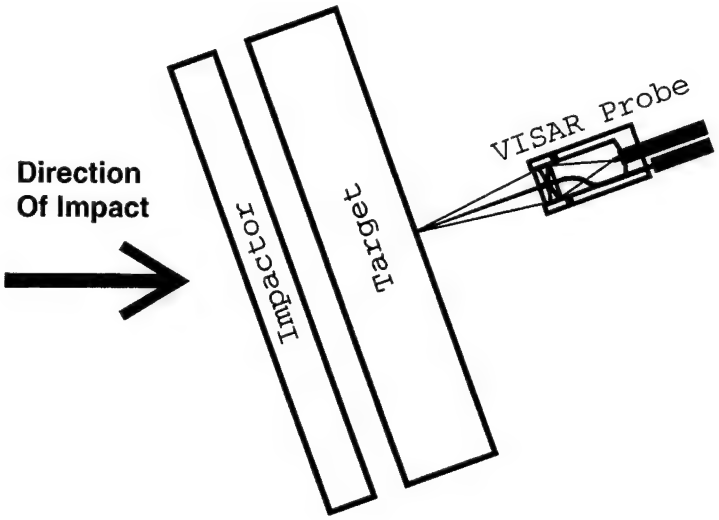

Figure 16. Oblique Impact Experiment Configuration.

By performing an oblique impact experiment at the same stress level as a comparable transmission experiment, the effects of the shear wave on shock properties can be monitored. Of particular interest is the effect of the shear wave induced deformation on the spall strength. Ti-6Al-4V is susceptible to shear banding (Bai et al. 1994). If shear band localization weakened the material prior to spallation, its effect would be observed from a change in the spall strength. Otherwise, the velocity profile should look identical to that of the transmission experiment.

The x-t and σ-u diagrams (Figures 17 and 18) are also similar to those of the transmission experiment. The shear wave travels through the material prior to a state of tension being developed. It is shown reaching the elastic release at point 6. Any significant effect caused by the shear wave should be observed in the spall signal. It is worth noting that these waves do not interact. The shear wave is placed in the x-t diagram only to illustrate the timing of events.

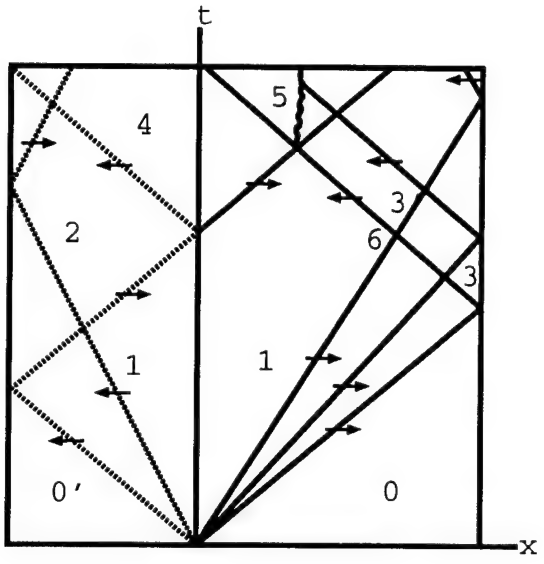

Figure 17. x-t Diagram (Oblique Impact).

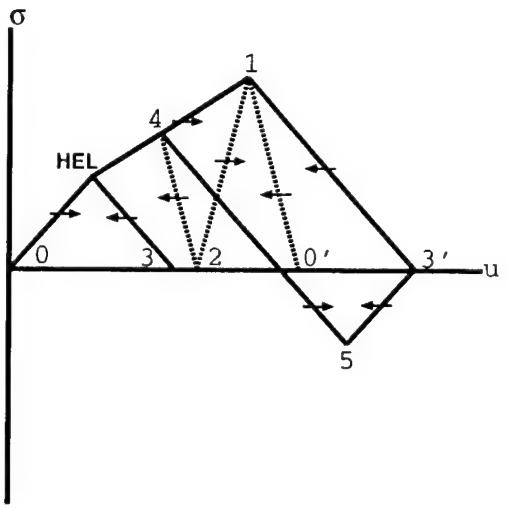

Figure 18. σ-u Diagram (Oblique Impact).

4. Results and Analysis

4.1 Elastic Constants. Density and ultrasonic sound speed measurements were taken on 21 samples of the low-cost Ti-6Al-4V alloy. These measurements were then used to calculate the material's elastic constants using the following equations (Schreiber et al. 1973):

$$L = \rho * U_l^2, \tag{1}$$

$$G = \rho * U_s^2, \tag{2}$$

$$K = \rho * (U_l^2 - ((4/3) * U_s^2)), \quad (3)$$

$$E = \rho * [(3 * U_l^2 * U_s^2) - (4 * U_s^4)] / (U_l^2 - U_s^2), \quad (4)$$

$$\lambda = \rho * (U_l^2 - (2 * U_s^2)), \quad (5)$$

and

$$\nu = [U_l^2 - (2 * U_s^2)] / [2 * (U_l^2 - U_s^2)], \quad (6)$$

where ρ = density, U_l = longitudinal wave speed, U_s = shear wave speed, L = longitudinal modulus, G = shear modulus, K = bulk modulus, E = Young's Modulus, λ = Lamé Constant, and ν = Poisson's Ratio.

The results of these calculations are shown in Table 1. Since the average values for density and sound speed are practically identical for both the aircraft/aerospace and low-cost alloys, the average values of the elastic constants follow suit. Also, specimens from shots no. 821, 823, and 837 are only used in this report as statistical data for density, sound speeds, and elastic constants.

4.2 Transmission Experiments. Six transmission experiments were performed to generate impact stresses from 4 to 13 GPa. These experiments provide information on the HEL, its dependence on specimen thickness, plastic deformation following the elastic precursor, and spall threshold. Pre-impact information for these experiments is given in Table 2. The values used for the elastic wave velocity and initial density are the measured values of longitudinal wave velocity and density for each individual Ti-6Al-4V specimen.

Figure 19 shows the recorded free surface velocity profiles. These profiles have been shifted in time for display purposes. This figure shows that the shock-compressed state in the titanium alloy is attained through the propagation of an elastic wave with the final shock state attained through the propagation of a slower shock wave. Using these profiles, measured values were obtained from the free surface velocity for the elastic and plastic velocity response, arrival time

Table 1. Elastic Constants of Ti-6Al-4V Specimens

Shot No.	ρ (g/cm^3)	U_l (mm/μs)	U_s (mm/μs)	L (GPa)	G (GPa)	K (GPa)	E (GPa)	λ (GPa)	ν (—)
821 (i)[a]	4.414	6.10	3.18	164	45	105	117	75	0.314
821 (t1)[b]	4.416	6.08	3.08	163	42	107	111	79	0.327
821 (t2)	4.416	6.11	3.10	165	42	108	113	80	0.326
823 (t1)	4.415	6.13	3.21	166	45	105	119	75	0.312
823 (t2)	4.417	6.06	3.11	162	43	105	113	77	0.321
827 (i)	4.408	6.19	3.23	169	46	108	121	77	0.314
830 (i)	4.412	6.16	3.21	167	45	107	119	76	0.313
832 (i)	4.414	6.16	3.23	167	46	106	120	75	0.311
832 (t1)	4.418	6.15	3.10	167	42	110	113	82	0.330
832 (t2)	4.414	6.16	3.28	168	48	104	124	72	0.302
836 (t)	4.418	6.12	3.22	166	46	105	120	74	0.309
837 (t)	4.423	6.15	3.09	168	42	111	112	83	0.332
847 (i)	4.415	6.12	3.19	165	45	105	118	75	0.313
847 (t)	4.418	6.09	3.22	164	46	103	119	72	0.306
848 (t)	4.415	6.17	3.13	168	43	111	115	82	0.327
850 (i)	4.419	6.08	3.11	164	43	107	113	78	0.323
850 (t)	4.419	6.09	3.17	164	44	105	117	75	0.314
907 (t)	4.418	6.13	3.20	166	45	106	119	76	0.313
912 (i)	4.409	6.10	3.05	164	41	109	109	82	0.333
912 (t)	4.406	6.10	3.23	164	46	102	120	72	0.304
922 (t)	4.414	6.11	3.16	165	44	106	116	76	0.317
Average	4.415 ± 0.008	6.12 ± 0.07	3.17 ± 0.13	165 ± 4	44 ± 4	106 ± 5	117 ± 8	77 ± 7	0.317 ± 0.018

[a] (i) = impactor material.
[b] (t#) = target material.

of the elastic wave at the free surface, arrival time of the elastic wave reverberation at the free surface, and the pull-back velocity for signals where spallation occurred. These values are listed in Table 3. Determination of these values allows the HEL, impact surface particle velocity, impact stress, plastic shock velocity, and density at the HEL to be calculated using equations 7–11.

These equations are based on the Rankine-Hugoniot jump conditions, which describe the conservation of mass, momentum, and energy:

$$u_e = V_e / 2, \tag{7}$$

Table 2. Transmission Experiments—Pre-Impact Information

Shot No.	Experimental Configuration (Impactor→Target)	Projectile Velocity (m/s)	Flyer Thickness (mm)	Target Thickness (mm)	Elastic Wave Velocity (Target) (km/s)	Initial Density (Target) (g/cm^3)
832A	T → T	653	3.954	5.993	6.15	4.418
832B	S → T	653	6.024	5.980	6.16	4.414
836	W → T	662	4.011	7.999	6.12	4.418
847	T → T	398	4.028	6.003	6.09	4.418
907	W → T	657	0.947	1.858	6.13	4.418
922	S → T	252	6.011	6.013	6.11	4.414

Note: T = low cost Ti-6Al-4V.
S = z-cut sapphire.
W = tungsten carbide.

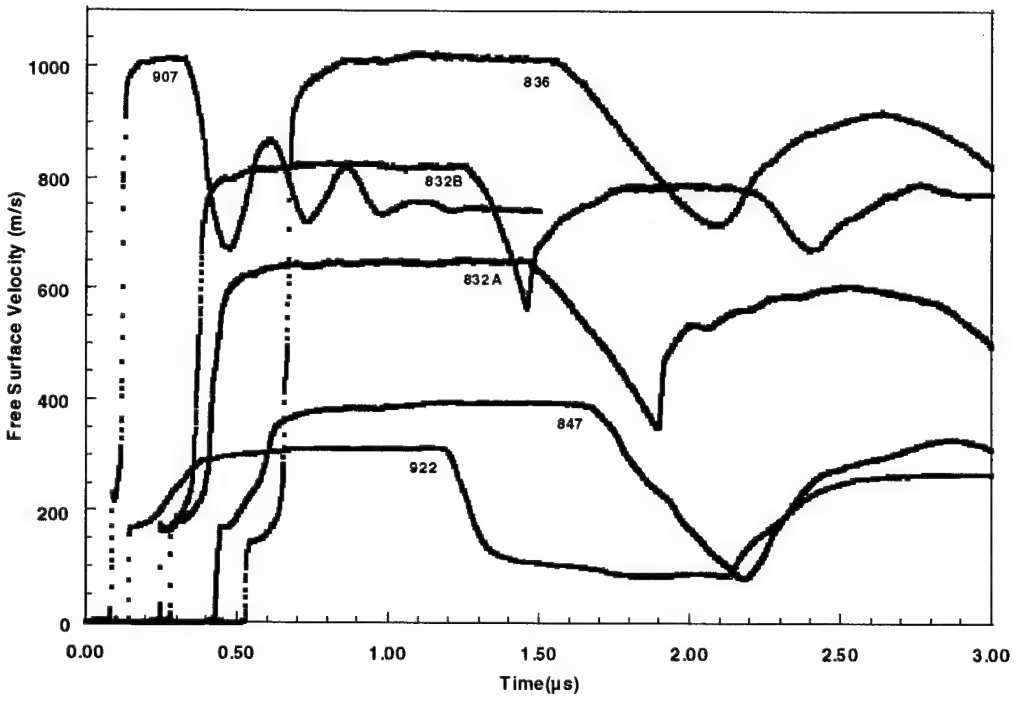

Figure 19. Free Surface Velocity Histories of Transmission Experiments.

Table 3. Measured Values Obtained From Transmission Experiments

Shot No.	Elastic Velocity Response (m/s)	Free Surface Velocity (m/s)	Elastic Wave Arrival Time (μs)	Reverberation Arrival Time (μs)	Pull-Back Velocity (m/s)
832A	172	653	1.276	1.417	306
832B	172	824	1.243	1.364	258
836	149	1022	1.525	1.658	298
847	173	394	1.421	1.574	314
907	218	1013	1.081	1.113	342
922	171	312	1.138	1.296	No Spall

$$HEL = u_e * (U_l * \rho_0), \tag{8}$$

$$U_p = (T_t - (((t_r - t_e)/2) * U_l)) / (((t_r - t_e)/2) + (T_t / U_l)), \tag{9}$$

$$\rho_e = \rho_0 / (1 - (u_e / U_l)), \tag{10}$$

and

$$\rho_i * (C_0 + (S * (u_p - V_p))) * (u_p - V_p) = HEL + (\rho_e * (U_p - u_e) * (u_p - u_e)), \tag{11}$$

where V_e = elastic particle velocity response, u_e = particle velocity at the HEL, U_l = elastic shock velocity, ρ_0 = initial density, U_p = plastic shock velocity, T_t = target thickness, t_e = elastic wave arrival time, t_r = reverberation arrival time, ρ_e = density at the HEL, ρ_i = impactor initial density, u_p = impact surface particle velocity, C_0 = impactor material coefficient, S = impactor material coefficient, V_p = projectile velocity, and U_i = impactor shock velocity.

The densities used for sapphire (Barker and Hollenbach 1970) and tungsten carbide (Karnes, unpublished data) were 3.98 and 14.85 g/cm^3, respectively. The respective shock velocities are 11.18 mm/μs and 6.9 mm/μs. Since the elastic wave release behavior is symmetric to its shock behavior, the particle velocity associated with the HEL is simply half of the elastic velocity response of the free surface. This velocity is then used to calculate the HEL by taking the

product of the particle velocity and material impedance. Plastic shock velocity is determined using the time difference of the elastic wave and its reverberations off of the plastic wave. Density at the HEL is calculated by using one of the Rankine-Hugoniot jump conditions. The impact surface velocity and stress are also determined by using the jump conditions. Since the stress state of the impactor and target are the same at the impact surface, equation 11 can be used to solve for the particle velocity at the impact surface. The velocity can then be put back into either side of the equation to solve for the impact stress. The left side of equation 11 represents a general impactor Hugoniot, which is different for every material. C_0 and S are material coefficients that describe linear shock behavior. Since three different impactor materials were used, their individual Hugoniots are supplied here. For the experiments using tungsten carbide impactors, a stress behavior of $[(-74.356 * (u_p - V_p)^2) - (105.44 * (u_p - V_p)) + 0.003]$ (Karnes, unpublished data) must be substituted to accurately predict the impact surface velocity and stress levels. This Hugoniot describes the elastic-plastic behavior of the tungsten carbide. Sapphire will be entirely elastic for the experiments in this report, and when used as an impactor will have a Hugoniot of $[-44.496 * (u_p - V_p)]$. For symmetric impacts, where the Ti-6Al-4V low-cost alloy is the impactor, $[\rho_i * (-U_i - V_p) * (u_p - V_p)]$ can be substituted for the Hugoniot. The results of these calculations are given in Table 4.

Table 4. Calculated Values Obtained From Transmission Experiments

Shot No.	HEL (GPa)	Target Thickness (mm)	Impact Surface Particle Vel. (m/s)	Impact Stress (GPa)	Plastic Shock Vel. (km/s)	Density at the HEL (g/cm^3)
832A	2.34	5.993	327	8.07	5.32	4.481
832B	2.34	5.980	418	10.43	5.44	4.476
836	2.02	7.999	524	13.13	5.53	4.472
847	2.33	6.003	197	4.91	5.21	4.482
907	2.95	1.858	519	13.12	5.51	4.498
922	2.31	6.013	161	4.06	5.20	4.477

One of the first interesting features of these results is the variation in the HEL. The amplitude of the elastic precursor appears to decay with propagation distance. This is evident from the profiles obtained in experiment nos. 836 and 907, which are shown in Figure 20. These experiments were performed to generate peak stresses of 13.1 GPa, and both reached roughly the

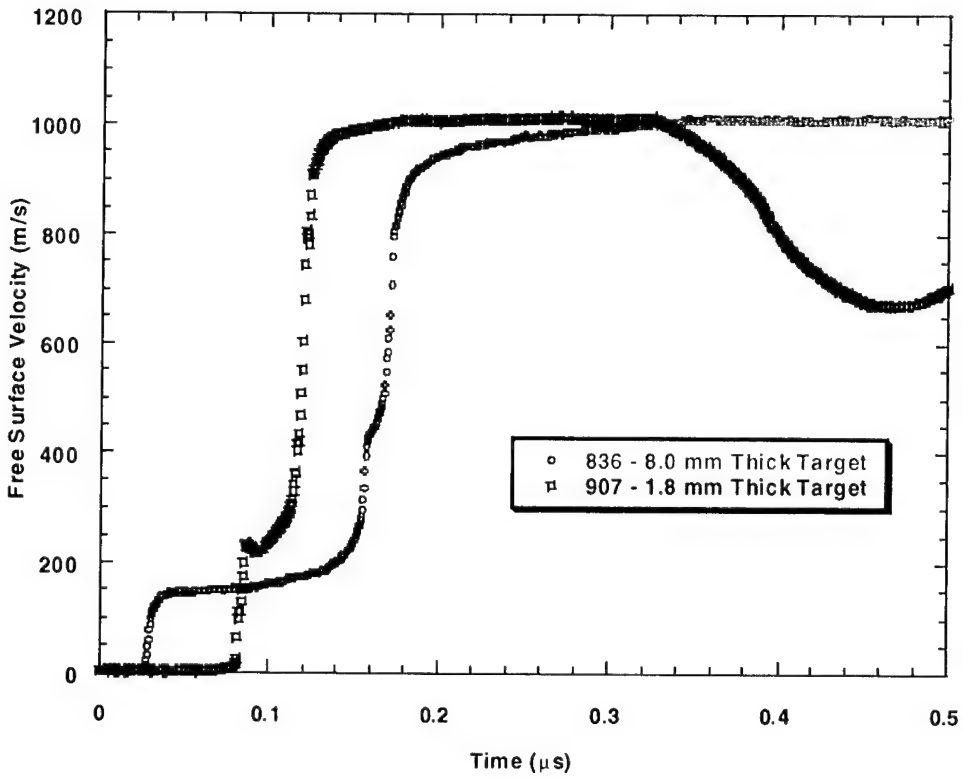

Figure 20. HEL Dependence on Material Thickness.

same peak velocity. Experimental configuration was identical, except for the thicknesses of the specimens. The targets used in these experiments were 8 mm and 1.8 mm thick, respectively. The value of the HEL varies between 2.02 and 2.95 GPa, which suggests that the value of the HEL is dependent on the thickness of the specimen. The uncertainty of these values is 1.2%.

Clean transitions between the elastic and plastic regions were evident for all of the experiments, except nos. 832A and 832B. The HELs of these experiments showed significant relaxation. As such, the HELs in these experiments were taken as the relaxed free surface velocity before the plastic rise. A plot of the HEL vs. target thickness is shown in Figure 21. All of the data points follow a linear pattern.

Velocity profiles obtained from these experiments do not show significant post yield hardening. The rise of the plastic region is fairly smooth with little ramping. If it is assumed

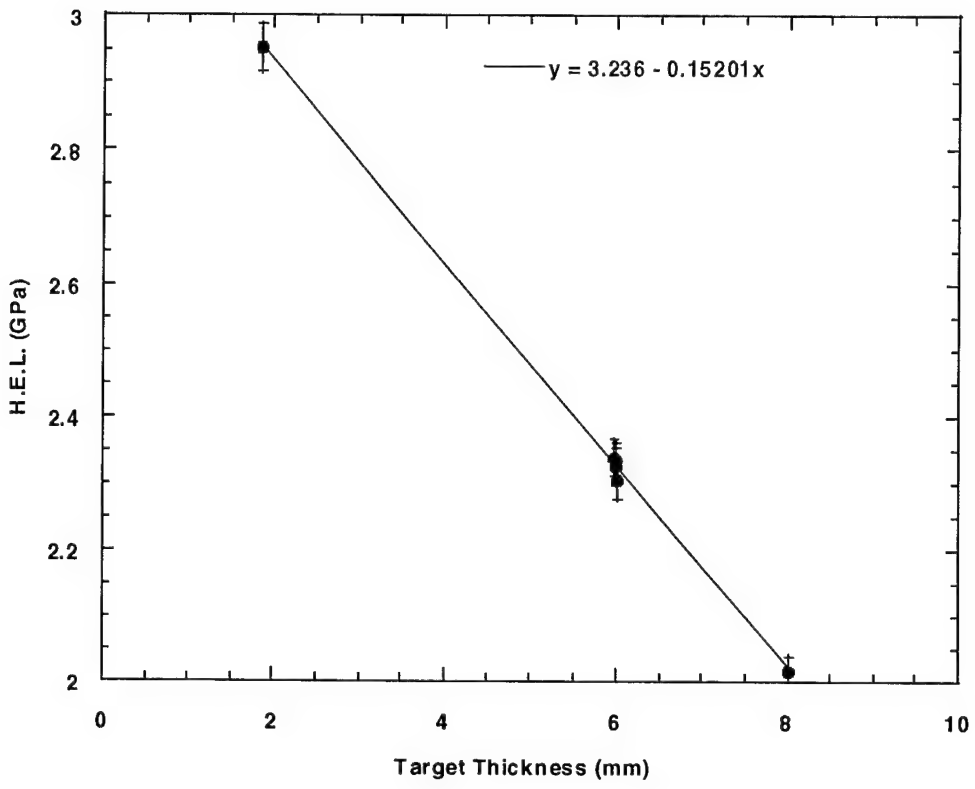

Figure 21. Elastic Precursor Decay With Thickness in Ti-6Al-4V.

that strain rate effects do not influence the magnitude of the HEL when an 8-mm-thick specimen is used, the dynamic yield stress is calculated by the following equation:

$$Y_d = (2 * U_s^2) / (U_l^2 * \sigma_{HEL}), \quad (12)$$

where Y_d = dynamic yield stress, σ_{HEL} = magnitude of HEL, U_l = longitudinal wave speed, and U_s = shear wave speed.

Y_d of the Ti-6Al-4V alloy was calculated as 1.09 GPa. This agrees well with the value of 1.15 GPa, determined by Weerasooriya (unpublished data) under compression at strain rates of 1300–3000 s^{-1}.

The plastic shock velocity following the elastic precursor varies between 5.20 and 5.53 km/s, with an average uncertainty that is less than 0.5%. This is the effective shock velocity relative to the particle velocity of the elastically deformed alloy, i.e., the particle velocity associated with the HEL. Figure 22 shows the calculated plastic wave velocities vs. their corresponding impact stresses. It is clear that the plastic shock velocity increases with stress.

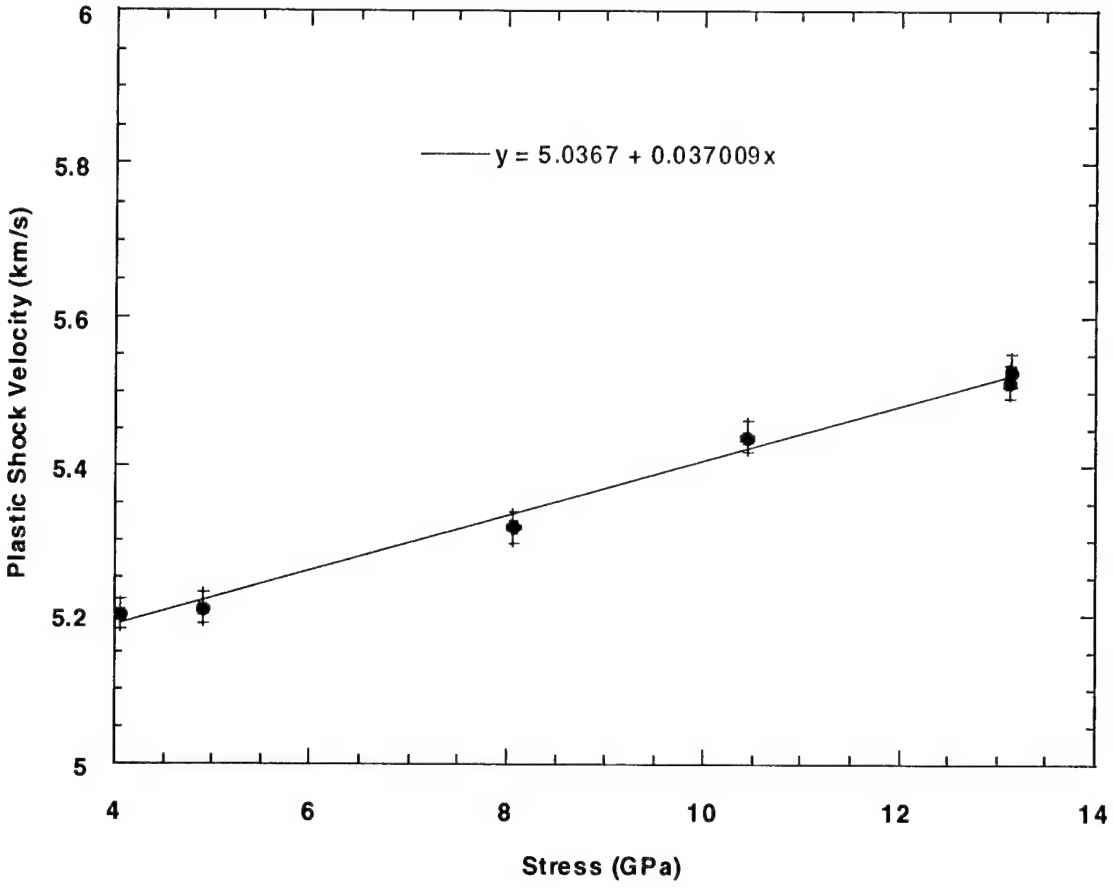

Figure 22. Plastic Shock Velocity vs. Impact Stress.

Usually, the arrival of the plastic shock in time is taken to be midway during the plastic rise. This value is then used with the elastic wave velocity to calculate the plastic shock speed. However, in this report, a more accurate technique was implemented. Once the elastic wave reaches the free surface of the target, it reflects back as a release wave and encounters the slower plastic wave. This encounter causes reverberations of the elastic wave to reflect between the

oncoming plastic wave and the free surface. If the arrival time of a reverberation can be identified, it can be used to determine the plastic shock velocity. Reverberations were identified in all of these experiments. An example of such a reverberation is evident as the large hump in the plastic rise of experiment no. 836 in Figure 20.

The magnitude of the plastic wave velocity is similar to the value of bulk sound speed (4.91 km/s) in the alloy. This implies that the alloy deforms plastically above the HEL (Graham and Brooks 1971). This inference is reinforced by calculating the free surface velocities on the assumption that the alloy deforms like an elastic-perfectly plastic material, and comparing them to measured values. An elastic-perfectly plastic material will release up to twice the stress level of the HEL elastically, with any remaining stress being released plastically. The observed and calculated free surface velocities vary by 1.5% on average (Table 5). Release impedance was calculated by dividing the impact stress by the difference in velocity of the free and impact surfaces. It was also dependent on stress, ranging from 24.7 to 26.9 Gg/m^2s.

Table 5. Plastic Response of Ti-6Al-4V

Shot No.	Calculated Free Surface Velocity (m/s)	Measured Free Surface Velocity (m/s)	% Difference (Absolute Value)	Release Impedance (Gg/m^2s)
832A	641	653	1.9	24.7
832B	827	824	0.3	25.7
836	1041	1022	1.8	26.4
847	381	394	3.4	24.9
907	1028	1013	1.5	26.6
922	312	312	0.1	26.9

Figure 23 shows the shock data obtained from the transmission experiments compared to the hydrodynamic compression curve. The hydrodynamic curve illustrates the response of isotropic material to equal compressive loading in all directions, and was calculated using shock data given by Morris et al. (1988) with equation 13. Equation 13 is valid for materials showing a linear relationship between its shock and particle velocities. The results of Morris et al. (1988) showed this to be true for Ti-6A1-4V alloy and the value of the slope was determined to be 1.06.

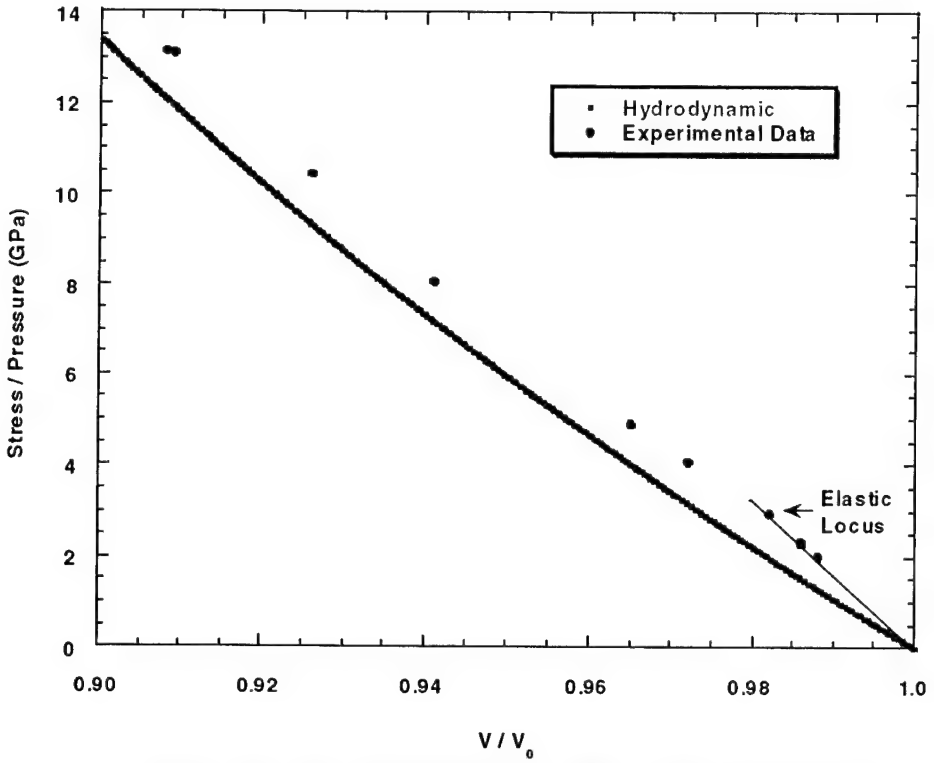

Figure 23. Shock Hugoniot and Hydrodynamic Curve.

Elastic/plastic behavior is evident from the change in the shock locus. The offset between the experimental data points and the hydrodynamic curve was used to calculate the material's shear strength using equation 14 (Jones and Graham 1971).

$$P = [\rho_0 * U_0^2 * \{1 - (\rho_0 / \rho_1)\}] / [1 - (s * \{1 - (\rho_0 / \rho_1)\})]^2, \quad (13)$$

and

$$\tau = 0.75 * (\sigma_1 - P), \quad (14)$$

where P = hydrodynamic pressure, ρ_0 = initial density, U_0 = bulk sound speed, $\rho 1$=final density, s = slope between shock and particle velocities, τ = shear stress, and σ_1 = impact surface stress.

Shear strength ranged from 0.60 to 0.90 GPa, increasing with stress (Table 6). Values for initial density, density at the HEL, and bulk sound speed are given previously in this work.

Table 6. Shear Strengths

Shot No.	Stress (GPa)	Final Density (g / cm^3)	V / V_0	P (GPa)	τ (GPa)
832A	2.34 / 8.07	4.481 / 4.693	0.986 / 0.941	1.54 / 7.17	0.60 / 0.67
832B	2.34 / 10.43	4.476 / 4.768	0.986 / 0.926	1.54 / 9.31	0.60 / 0.84
836	2.02 / 13.13	4.472 / 4.868	0.988 / 0.908	1.31 / 12.08	0.53 / 0.79
847	2.33 / 4.91	4.482 / 4.579	0.986 / 0.965	1.54 / 4.03	0.59 / 0.66
907	2.95 / 13.12	4.498 / 4.859	0.982 / 0.909	1.99 / 11.92	0.72 / 0.90
922	2.31 / 4.06	4.477 / 4.543	0.986 / 0.972	1.54 / 3.17	0.58 / 0.67

Densities caused by the plastic wave were calculated using the previously mentioned jump conditions. The volumetric ratio, V/V_0, was determined using the initial and final densities of both the elastic and plastic response. The left value of each column corresponds to the elastic response while the right value reflects the states attained by the plastic wave.

Spall strength was also monitored during these experiments, and was taken as the product of plastic impedance and half the magnitude of the pull-back velocity. It varied from 3.1 to 4.2 GPa (Table 7) with an average precision of 5.6%. The pulse widths of these experiments ranged from 1.1 to 1.3 μs with the exception of experiment no. 907, which had a pulse width of 0.274 μs. Spall strength dependence on pulse width is shown by a comparison of experiment nos. 836 and 907 in Figure 24. These experiments were identical, except for the specimen thicknesses used. However, large differences exist in the signal pull-back velocities, leading to respective spall strengths of 3.7 and 4.2 GPa for experiment nos. 836 and 907.

Secondary spall resistance, as described by Johnson et al. (1996), was also observed in the velocity profiles of the Ti-6Al-4V alloy and verified through recovery of the targets. It can be seen in experiment no. 847, as shown in Figure 25, as the sharp deceleration in the velocity return after the pull-back signal. Secondary spall resistance occurs when the spall fracture surface is not a smooth plane, but a series of cracks that span hundreds of micrometers. Separation of the material causes the formation of new, interconnecting cracks, which provide the secondary spall resistance. A micrograph of the recovered target from experiment no. 847 is

Table 7. Spall Thresholds

Shot No.	Impact Stress (GPa)	Pulse Width (μs)	Pull-Back Velocity (m/s)	Spall Strength (GPa)
832A	8.07	1.285	306	3.7
832B	10.43	1.078	258	3.1
836	13.13	1.163	298	3.7
847	4.91	1.325	314	3.7
907	13.12	0.274	342	4.2
922	4.06	1.075	No Spall	No Spall

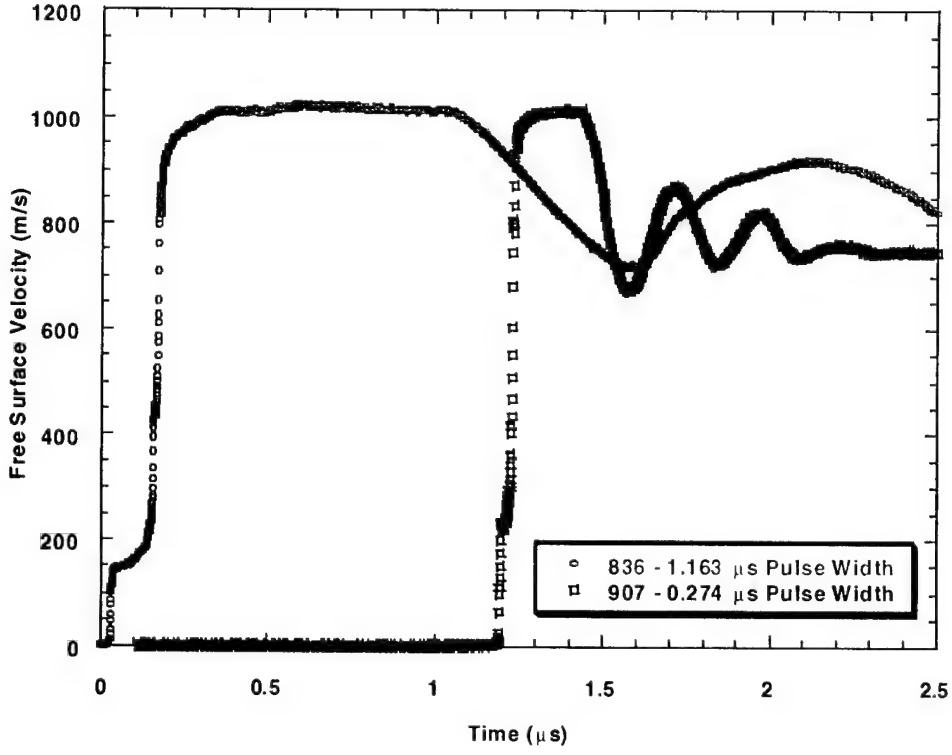

Figure 24. Spall Strength Dependence on Pulse Width.

shown in Figure 26. The spall cracks in this specimen span over 1 mm of the target thickness. Lastly, in experiment no. 922, Ti-6Al-4V did not spall. This was an expected result, as the level of tension pulled by the release wave interaction was only 2.61 GPa.

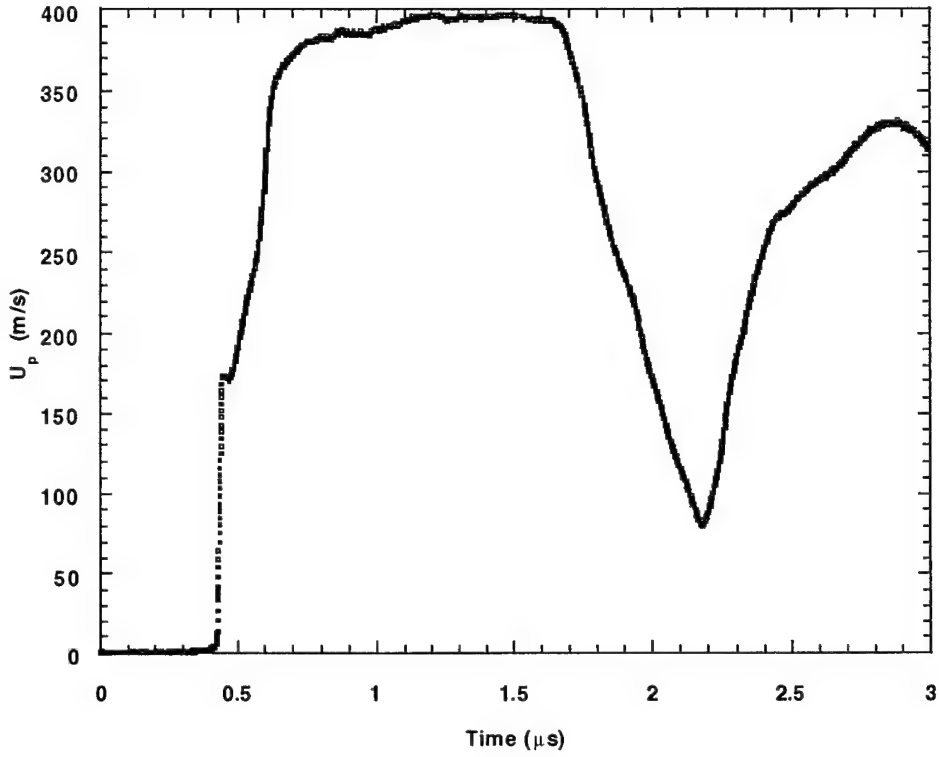

Figure 25. Secondary Spall Resistance.

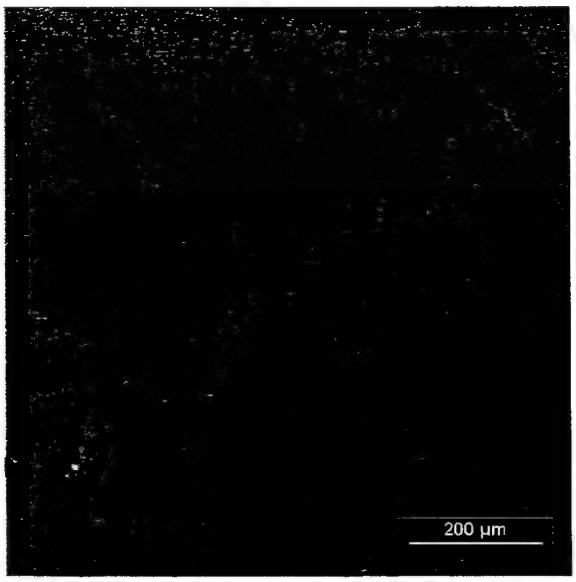

Figure 26. Secondary Spall Resistance Cracking in Experiment No. 847.

4.3 Direct Impact Experiments. Two direct impact experiments were performed at impact stress levels of 10.5 and 13.5 GPa. These experiments provide additional information on the initial shock and the release behavior of the new Ti-6Al-4V alloy. The pre-impact measurements from these experiments are listed in Table 8.

Table 8. Direct Impact Experiments—Pre-Impact Information

Shot No.	Experimental Configuration (Impactor→ Target)	Flyer Thickness (mm)	Target Thickness (mm)	Projectile Velocity (m/s)	ElasticWave Velocity (km/s)	Initial Density (g/cm^3)
827	T → W	7.997	0.934	656	6.19	4.408
830	T → S	8.039	2.081	654	6.16	4.412

Note: T = low cost Ti-6Al-4V.
S = z-cut sapphire.
W = tungsten carbide.

The velocity traces obtained from these experiments are shown in Figure 27. Individual velocity jumps at the free surface were measured and used to calculate the shock and release states at the impact surface. Measured free surface values are listed in Table 9. Only the first few jumps from each experiment were used in the analysis of the release behavior, as later jumps occurred outside a state of uniaxial strain. Subsequent jumps in velocity also became too small for accurate calculations.

The first jump is caused by the release of the impact stress at the free surface. Subsequent jumps are caused by reverberations of the release wave, which reflect back as shocks upon reaching the higher impedance impactor, and again release at the free surface.

The shock response of the tungsten carbide and sapphire used in these experiments are well characterized. Z-cut sapphire, used in experiment no. 830 remains elastic for the stress levels seen here. As such, its shock and release behavior are identical. This fact is used to calculate the impact surface velocities and stress levels with the following equations.

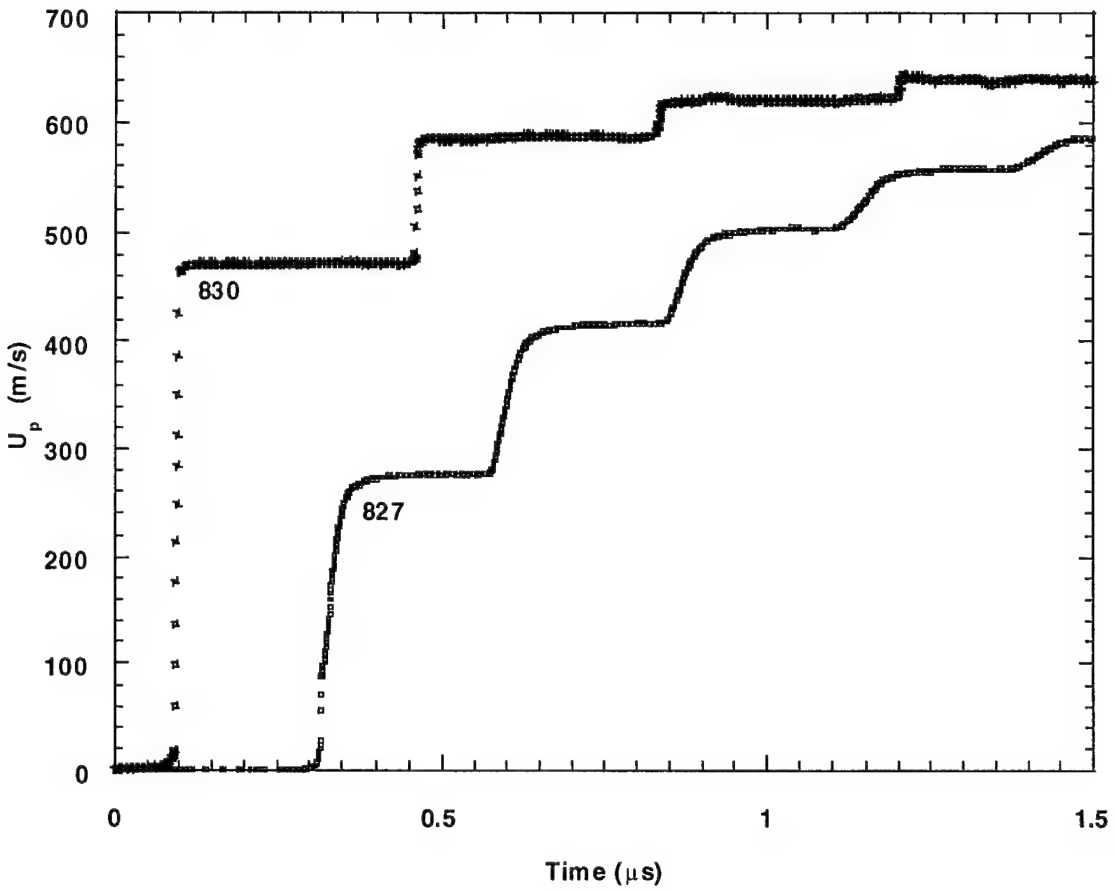

Figure 27. Free Surface Velocity Histories of Direct Impact Experiments.

Table 9. Direct Impact Experiment Measurements

Shot No.	Velocity Jump 1 (m/s)	Velocity Jump 2 (m/s)	Velocity Jump 3 (m/s)	Velocity Jump 4 (m/s)
827	274	417	503	557
830	471	587	621	—

$$u_p = [(v_f - v_i) / 2] + v_i, \quad (15)$$

and

$$\sigma_p = 44.496 * [(v_f - v_i) / 2], \quad (16)$$

where u_p = impact surface velocity, vi = pre-jump velocity, σ_p = impact surface stress, and v_f= post-jump velocity.

Tungsten carbide has been reported (Karnes, unpublished data) as having different shock and release behaviors for the stress levels seen here. However, assuming identical behavior for the shock and release produced results that matched those of the transmission experiments. As such, the impact surface velocities of experiment no. 827 were also calculated using equation 15. Stress levels of the tungsten carbide were determined using equation 17:

$$\sigma_p = [-74.356 * ((v_f - v_i) / 2)^2] + [105.440 * ((v_f - v_i) / 2)] + 0.003. \quad (17)$$

The results of both direct impact experiments are shown in Table 10. The initial impact surface velocities and stresses matched the data from similar transmission experiments, varying by only 0.5%.

Hugoniot data is typically used to describe the behavior of a material that is shocked from a rest state. The Ti-6Al-4V samples used during these experiments were impactors. As such, "Equivalent Target" velocities were calculated. These are the equivalent velocities that would have been reached by a Ti-6Al-4V target material at the same stress levels, and were calculated by taking the difference of the projectile velocity and the impact surface velocities. Release impedances were calculated between successive points on the release path as the difference in impact stress divided by the difference in stationary velocity. The values shown here are similar to the release impedances calculated from the transmission experiments. Shock and release Hugoniot points are shown in Figure 28, for both the transmission and direct impact experiments. The separation of the data becomes greater at the lower stress levels. This is expected, as the transmission experiments are shocked elastically initially, while the direct impact experiments are releasing near plastically at the lower stress levels.

4.4 Re-Shock Experiments. Two re-shock experiments were performed, generating re-shock stresses of 10.4 and 20.4 GPa off of the initial shock. These experiments provide insight into the behavior of the Ti-6Al-4V alloy at increased stress levels, after the material has been

Table 10. Release Behavior of Direct Impact Experiments

Shot No.	Impact Surface Velocity (m/s)	"Equivalent Target" Velocity (m/s)	Impact Surface Stress (GPa)	Release Impedance (Gg/m^2s)
827	137	519	13.05	—
827	346	311	7.16	28.3
827	460	196	4.40	24.1
827	530	126	2.80	22.9
830	236	419	10.48	—
830	529	125	2.58	26.9
830	604	50	0.76	24.3

previously shocked. Pre-impact information is shown for both experiments in Table 11. Velocity profiles obtained for these experiments are shown in Figure 29.

The first two velocity jumps correspond to the free surface release of the interactions between the Ti-6Al-4V target's elastic and plastic waves and target 2. Assuming that both the tungsten carbide and sapphire have the same shock and release behavior for the stress levels seen here, the velocity of the re-shock interface is simply one half the velocity of the jumps. The particle velocity reached by the interaction of the elastic wave at the re-shock interface (state 2 of Figure 14) is one half the first jump level. The particle velocity reached by the interaction of the plastic wave at the re-shock interface (state 4) is one half the second jump level. Equations 16 and 17 can again be used to determine the stress levels for the sapphire and tungsten carbide respectively. The pre-jump velocities for both the elastic and plastic wave calculations would be zero. The results of these calculations are listed in Table 12, along with the jump measurements.

Once the re-shock states at the target 1/target 2 interface have been determined, the HEL and re-shock impedance may be calculated. The initial shock behaviors of the impactor and target 1 have been previously determined in the transmission experiments. Experiment no. 832A had essentially the same impact configuration and projectile velocity as experiment no. 912. Similarly, experiment no. 907 closely matched experiment no. 848. As such, the particle velocity and stress levels of the impact surface, and the shock speeds of the Ti-6Al-4V are easily determined.

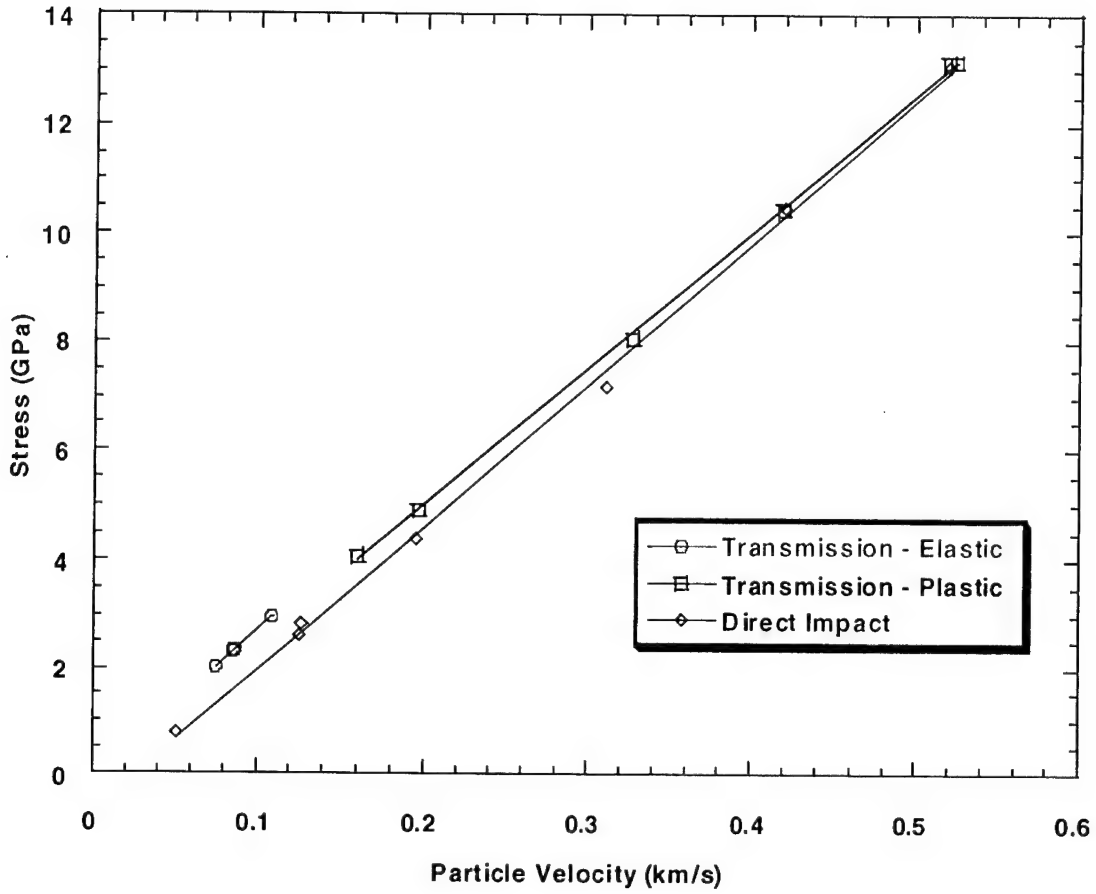

Figure 28. Transmission and Direct Impact Data.

Table 11. Re-Shock Experiments—Pre-Impact Information

Shot No.	Experimental Configuration (Impactor → Target)	Flyer Thickness (mm)	Target Thickness (mm)	Projectile Velocity (m/s)	Elastic Wave Velocity (km/s)	Initial Density (g/cm^3)
848	W → T + W	5.982	2.054 / 0.918	644	6.17	4.415
912	T → T + S	7.956	6.269 / 1.022	656	6.10	4.406

Note: T = low cost Ti-6Al-4V.
S = z-cut sapphire.
W = tungsten carbide.

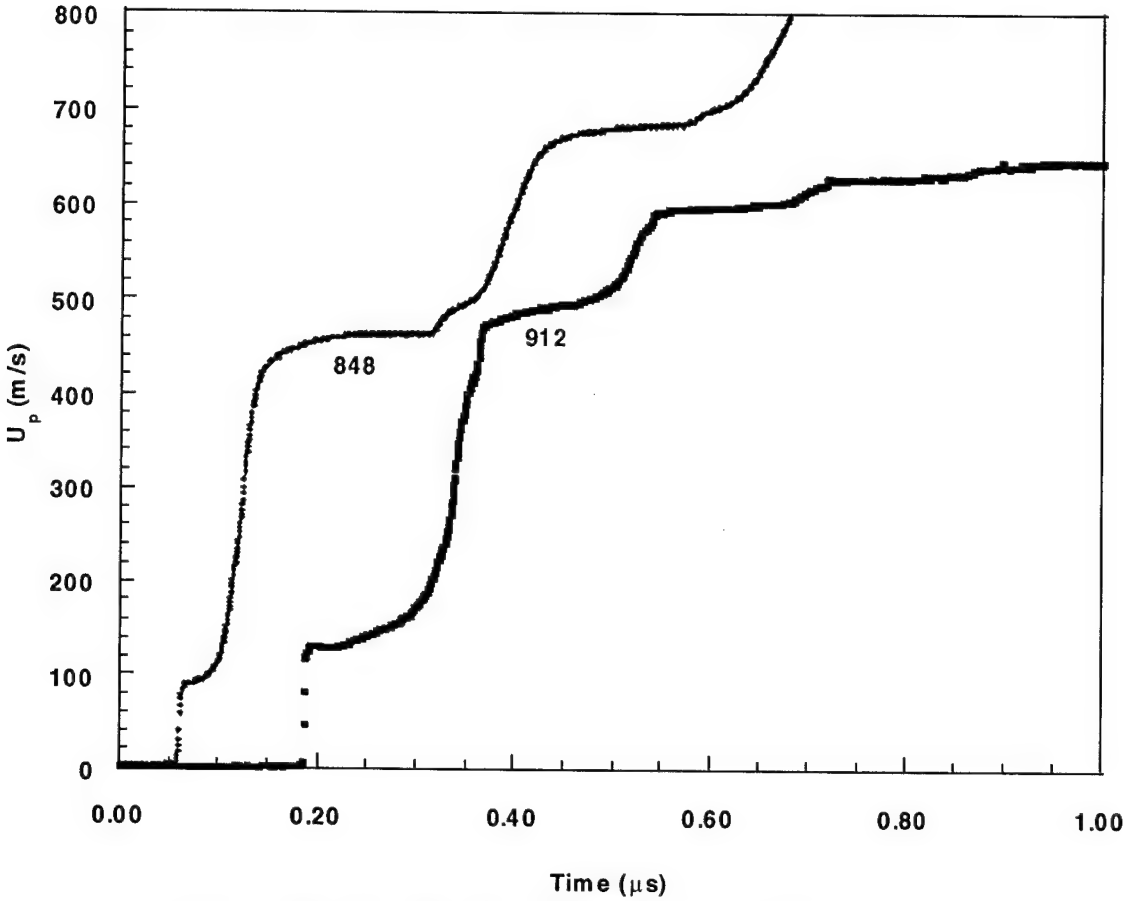

Figure 29. Velocity Histories of Re-Shock Experiments.

Table 12. Re-Shock States

Shot No.	1st Jump Velocity (m/s)	Particle Velocity (state 2) (m/s)	Stress (state 2) (GPa)	2nd Jump Velocity (m/s)	Particle Velocity (state 4) (m/s)	Stress (state 4) (GPa)
848	91	46	4.65	464	232	20.46
912	130	65	2.89	472	236	10.50

The HEL occurs at the intersection of the elastic and plastic impedance locus. Since the slope of these lines is already known (based on the respective impedances from experiments no. 832A and 907), only one point on each line is required to determine their intersection. The initial state (zero velocity and zero stress) lies on the elastic impedance line, while the particle velocity and stress reached by the elastic wave's re-shock lie on the plastic line. This information was used to calculate the HELs for both re-shock experiments. Predicted values for the HEL were taken from Figure 21, using the thickness of target 1. As shown in Table 13, the difference in these values is small. This supports the results of the transmission experiments, which show that the HEL varies with specimen thickness.

Table 13. Re-Shock Experiments HELs and Impedances

Shot No.	Calculated HEL (GPa)	Predicted HEL (GPa)	% Difference	"Equivalent Target" Velocities (m/s)	Re-Shock Impedances (Gg/m^2s)
848	3.02	2.92	3.2	786	27.4
912	2.35	2.28	3.1	420	26.3

Re-shock impedance was calculated using the impact stress and velocity from experiment nos. 832A and 907. These are the initial shock conditions. However, as in the direct impact experiments, Hugoniot data is reported for the target material. As such, "Equivalent Target" velocities were calculated for the plastic re-shock response of both experiments. In the re-shock experiment, as shown in Figure 13, the re-shock occurs in the opposite direction of the initial shock. The "Equivalent Target" velocity is, therefore, the difference between the impact surface and re-shock surface velocities added to the impact surface velocity. Once the "Equivalent Target" velocities have been determined, the re-shock impedance is simply the difference in stress between the same two points divided by the difference in velocity. These results are shown in Table 13. The re-shock impedances are significantly higher than the plastic impedances seen in experiment nos. 832A and 907. This suggests that the initial shocks may have caused some work hardening in the material. Further investigation is required to confirm this. Figure 30 shows a plot of stress vs. particle velocity, and includes data points from the transmission and re-shock experiments.

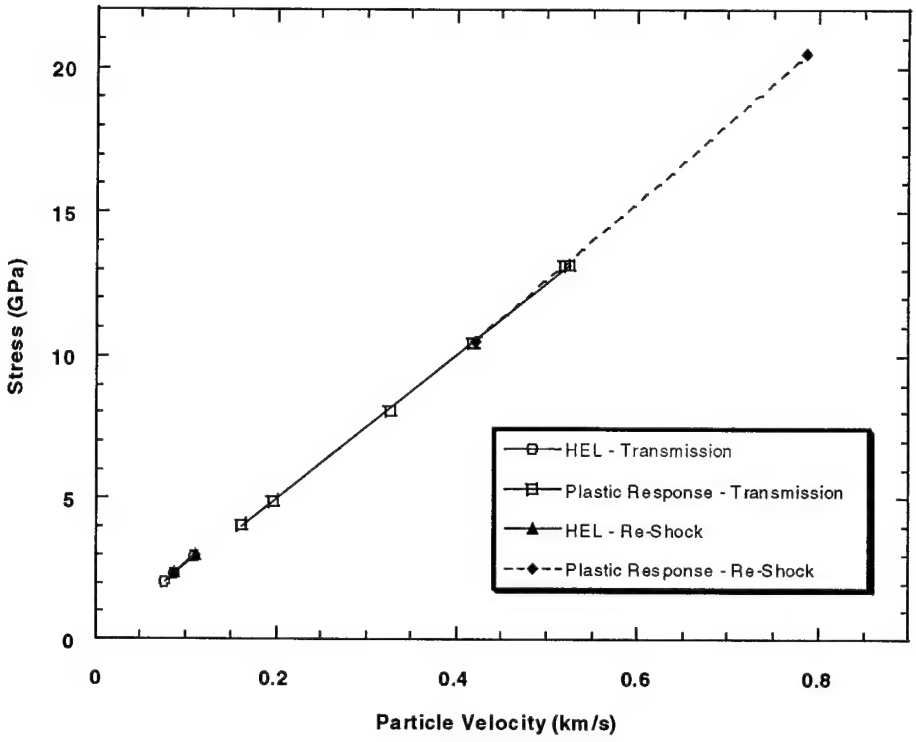

Figure 30. Transmission and Re-Shock Data.

4.5 Oblique Impact Experiments. As mentioned earlier, Ti-6Al-4V is susceptible to shear banding (Bai et al. 1994). In an effort to gauge the susceptibility of the new alloy to shear banding and its effect on spall strength, an oblique impact experiment was performed. The obliquity of impact in experiment no. 850 was 19°53′. An impact velocity of 423 m/s was used. This velocity would create the same impact velocity and stress levels as in the normal impact of experiment no. 847. The pre-impact information for both experiments is listed in Table 14. The specimen thicknesses used allowed the shear wave to pass through the area where the spall plane would form prior to a state of tension being developed.

Figure 31 shows the velocity profiles for both experiments. It is evident from this plot that both targets exhibit the same behavior. The HEL, peak velocity, plastic shock speed, and pull-back velocity are virtually identical. Both samples also exhibit secondary spall resistance.

Table 14. Experiment Nos. 847 and 850 Pre-Impact Information

Shot No.	Experimental Configuration (Impactor → Target)	Flyer Thickness (mm)	Target Thickness (mm)	Projectile Velocity (m/s)	Elastic Wave Velocity (Target) (km/s)	Initial Density (Target) (g/cm^3)
847	T → T	4.028	6.003	398	6.09	4.418
850	T → T (at 19°53′)	4.031	6.011	423	6.09	4.419

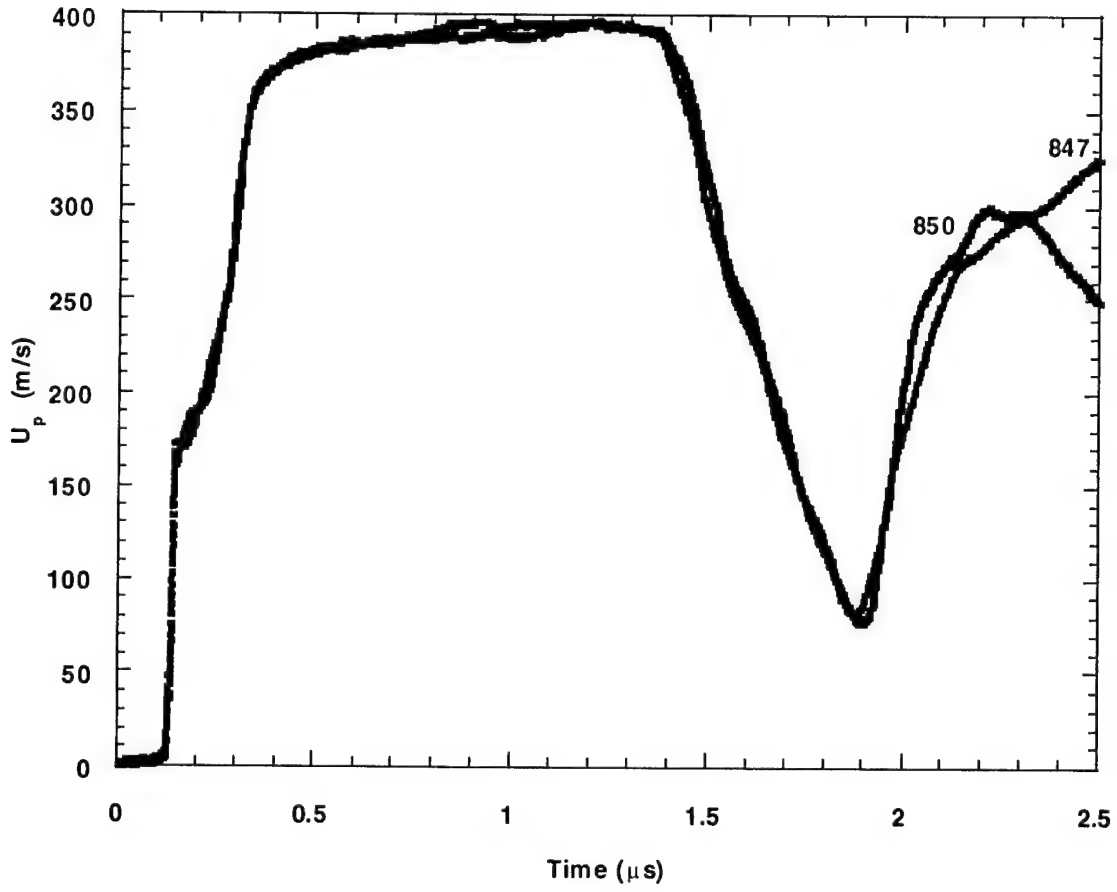

Figure 31. Free Surface Velocity Histories of Experiment Nos. 847 and 850.

The effect of the shear wave on spall strength was nonexistent. Furthermore, examination of the recovered target revealed the same type of cracking associated with secondary spall resistance (Figure 32) as that found in experiment no. 847. Shear bands were also not present.

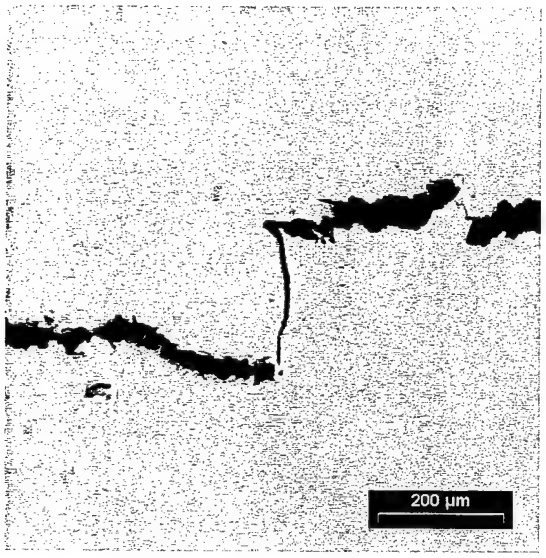

Figure 32. Secondary Spall Resistance Cracking in Experiment No. 850.

Measured and calculated values for both experiments are shown in Tables 15, 16, and 17. The differences are insignificant in the recovered material. As such, for an impact stress level of 4.9 GPa and an impact angle of 20°, increased shear deformation does not appear to affect the spall strength of the Ti-6Al-4V alloy or cause the formation of shear bands.

4.6 Comparison. As many investigators have studied Ti-6Al-4V, substantial information is available to compare to the shock response of the low-cost alloy. The authors of this report assume that all materials studied in the previous works were of aircraft/aerospace quality. The compiled properties of the aircraft/aerospace alloy are shown in Table 18.

The elastic behaviors of the two alloys are similar. The aircraft/aerospace alloy has an HEL ranging from 2.0–2.8 GPa, while the HEL of the low-cost alloy ranges from 2.0–3.0 GPa. However, no mention of elastic precursor decay with material thickness was found in any of the previous works. Shock compression beyond the HEL in both materials was attained through plastic deformation.

Differences were reported in the shear strengths of the two materials. Hopkins and Brar (2000) reported that shear strength increased with increasing stress, ranging from 0.9 GPa at the

Table 15. Measured Values Obtained From Experiment Nos. 847 and 850

Shot No.	Elastic Velocity Response (m/s)	Free Surface Velocity (m/s)	Elastic Wave Arrival Time (μs)	Reverberation Arrival Time (μs)	Pull-Back Velocity (m/s)
847	173	394	1.421	1.574	314
850	175	390	1.700	1.853	316

Table 16. Calculated Values Obtained From Experiment Nos. 847 and 850

Shot No.	HEL (GPa)	Impact Surface Particle Velocity (m/s)	Impact Stress (GPa)	Plastic Shock Velocity (km/s)	Density at the HEL (g/cm^3)
847	2.33	197	4.91	5.21	4.482
850	2.36	195	4.87	5.22	4.483

Table 17. Spall Thresholds

Shot No.	Impact Stress (GPa)	Pulse Width (μs)	Pull-Back Velocity (m/s)	Spall Strength (GPa)
847	4.91	1.325	314	3.67
850	4.87	1.325	316	3.69

HEL to 1.6 GPa at a stress level of 12.5 GPa. These values were obtained through simultaneous measurements of longitudinal and lateral stresses. The low-cost alloy's shear strength also increased with stress, ranging from 0.5 GPa at the HEL to 0.9 GPa at a stress level of 13.1 GPa.

Spall strength values also varied between the two materials. Good agreement exists between the spall strengths reported by Kanel and Petrova (1981) and Andriot et al. (1994), and those of the low-cost alloy. The range of values reported by Me-Bar et al. (1987), Froeschner et al. (1989), and Chhabildas et al. (1990) are higher than those of the low-cost alloy. Me-Bar et al. (1987) reported that the initial microstructure of the alloy did not influence spall strength.

Table 18. Compiled Properties of Ti-6Al-4V

Authors	Pulse Width (μs)	Impact Stress (GPa)	HEL (GPa)	Spall Strength (GPa)	Shear Strength (GPa)
Morris et al. (1988)	—	—	2.8	—	—
Kanel and Petrova (1981)	—	—	2.0	3.4	—
Me-Bar et al. (1987)	1.2	10.5	—	4.1–5.0	—
Froeschner et al. (1989)	0.15	—	—	4.7–4.9	—
Chhabildas et al. (1990)	1.0	13.6	2.3	5.1	—
Andriot et al. (1994)	1.0	52–64	2.8	3.6–4.2	—
Hopkins and Brar (2000)	—	12.5	2.7	—	0.9–1.6

Variations in pulse width (Table 18) also do not explain the differences in the values of spall threshold. However, the results of the present work indicate that spall strength is pulse dependent.

5. Conclusions

A low-cost Ti-6Al-4V alloy of similar composition and microstructure to the presently used aircraft/aerospace alloy has been characterized up to stress levels of 20 GPa. Transmission experiments showed that the alloy, as with the more expensive material, exhibited elastic-plastic behavior. The elastic precursor, or HEL, varied from 2.0–3.0 GPa and was dependent on specimen thickness. Plastic shock velocity ranged from 5.2–5.5 km/s and was dependent on stress level. Release of the free surface also indicated elastic-plastic behavior. Shear strength increased with stress level and varied from 0.5–0.9 GPa. Spall strength varied with pulse width and ranged from 3.1–4.2 GPa. Secondary spall resistance was also observed in the velocity profiles and verified through examination of recovered samples.

Direct impact experiments mapped out the initial shock and subsequent release behavior of the material. Release impedances obtained were similar to those of the transmission experiments. They also confirm the elastic-plastic behavior of the material.

Re-shock experiments were used to characterize the material behavior at higher, post-shock stress conditions. Values of the HEL and plastic shock impedance were higher than those of the transmission experiments. This suggests that the initial shock caused the material to work harden. The experiments also confirm the HELs dependence on specimen thickness and elastic-plastic behavior.

An oblique impact experiment was performed to monitor the effects of increased shear deformation on spall strength. The results of the oblique impact closely matched those of a transmission experiment at similar stress levels. No significant differences were observed between the two experiments. Recovered samples from both experiments showed the same microstructure and cracking behavior. Shear banding was not observed in either sample.

A comparison of the aircraft/aerospace and low-cost alloys revealed similar shock behavior. The HEL of both materials was similar, and both materials exhibited elastic-plastic behavior. Shear strengths of both alloys increased with increasing stress levels. However, the ranges of shear strength of the two alloys varied considerably. Spall strength ranges of the two materials also showed considerable variations.

7. References

Andriot, P., P. Lalle, and J. P. Dejean. "Quasi-Elastic Behavior of Pure Titanium and TA6V4 at High Pressure." *High Pressure Science and Technology 1993,* p. 1009, edited by S. C. Schmidt, J. W. Shaner, G. A. Samara, and M. Ross, New York, NY: American Institute of Physics, 1994.

Asay, J. R., L. C. Chhabildas, and D. P. Dandekar. "Shear Strength of Shock-Loaded Polycrystalline Tungsten." *Journal of Applied Physics,* vol. 51, pp. 4774–4783, 1980.

Barker, L. M., and R. E. Hollenbach. "Shock-Wave Studies of PMMA, Fused Silica, and Sapphire." *Journal of Applied Physics,* vol. no. 41, pp. 4208–4426, 1970.

Bai, H., D. Qingdong, H. Changsheng, W. Desheng, and H. Haibo. "Micro-Analysis of Adiabatic Shear Fracture in Explosive-Filled Cylinders." *High Pressure Science and Technology 1993,* pp. 1229–1232, edited by S. C. Schmidt, J. W. Shaner, G. A. Samara, and M. Ross, New York, NY: American Institute of Physics, 1994.

Burkins, M., M. G. Wells, J. Fanning, and B. Roopchand. "The Mechanical and Ballistic Properties of an Electron Beam Single Melt of Ti-6Al-4V Plate." U.S. Army Research Laboratory, Aberdeen Proving Ground, MD, to be published.

Chhabildas, L. C., L. M. Barker, J. R. Asay, and T. G. Trucano. "Spall Strength Measurements on Shock Loaded Refractory Metals." *Shock Waves in Condensed Matter 1989,* pp. 429–432, edited by S. C. Schmidt, J. N. Johnson, and L. W. Davison, New York, NY: North-Holland, 1990.

Froeschner, K. E., D. E. Maiden, and H. H. Chau. "Spall Due to Short High Intensity Impulses." *Journal of Applied Physics,* vol. 65, pp. 2964–2973, 1989.

Graham, R. A., and W. P. Brooks. "Shock-wave Compression of Sapphire from 15 to 420 kbar. The Effects of Anisotropic Compressions." *Journal of Physics and Chemistry of Solids,* vol. 32, pp. 2311–2330, 1971.

Hemsing, W. F. "Velocity Sensing Interferometer (VISAR) Modification." *Review of Scientific Instruments.,* vol. 50, pp. 73–78, 1979.

Hopkins, A., and N. S. Brar. "Hugoniot and Shear Strength of Titanium 6-4 Under Shock Loading." *Shock Compression of Condensed Matter–1999,* pp. 423–426, edited by M. D. Furnish, L. C. Chhabildas, and R. S. Hixon, American Institute of Physics, NY, 2000.

Johnson, J. N., R. S. Hixson, D. L. Tonks, and A. K. Zurek. "Rate Dependent Spallation Properties of Tantalum." *Shock Compression of Condensed Matter 1995,* edited by S. C. Schmidt and W. C. Tao, New York, NY: American Institute of Physics, 1996.

Jones, O. E., and R. A. Graham. "Shear Strength Effects on the Phase Transition 'Pressures,' Determined From Shock-Compression Experiments." *Accurate Characterization of the High Pressure Environment 1968,* pp. 229–242, edited by E. C. Lloyd, 1971.

Kanel, G. I., and E. N. Petrova. "The Strength of Titanium BT6 at Shock-Wave Loading." *II Workshop on Detonation (USSR)*, pp. 136–142, Chergnogolovka, USSR, 1981.

Karnes, C. Sandia National Laboratory, Albuquerque, NM. Unpublished data.

Lysne, P. C., C. M. Percival, R. R. Boade, and O. E. Jones. *Journal of Applied Physics,* vol. 40, p. 3786, 1969.

Me-Bar, Y., M. Boas, and Z. Rosenberg. *Material Science and Engineering,* vol. 85, pp. 77–84, 1987.

Morris, C. E., M. A. Winkler, and A. C. Mitchell. "Ti-6Al-4V Alloy Wave Profile Measurements in the Shadow Region." *Shock Waves in Condensed Matter 1987,* pp. 265–268, edited by S. C. Schmidt and N. C. Holms, New York, NY: North-Holland, 1988.

Papadakis, E. P. "Ultrasonic Phase Velocity by the Pulse-Echo-Overlap Method Incorporating Diffraction Phase Corrections." *The Journal of the Acoustical Society of America*, vol. 42, pp. 1045–1051, 1967.

Schreiber, E., O. L. Anderson, and N. Soga. *Elastic Constants and Their Measurements*. New York, NY: McGraw-Hill Inc., 1973.

Weerasoriya, T. U.S. Army Research Laboratory, Aberdeen Proving Ground, MD. Unpublished data.

NO. OF COPIES	ORGANIZATION
2	DEFENSE TECHNICAL INFORMATION CENTER DTIC DDA 8725 JOHN J KINGMAN RD STE 0944 FT BELVOIR VA 22060-6218
1	HQDA DAMO FDT 400 ARMY PENTAGON WASHINGTON DC 20310-0460
1	OSD OUSD(A&T)/ODDDR&E(R) R J TREW THE PENTAGON WASHINGTON DC 20301-7100
1	DPTY CG FOR RDA US ARMY MATERIEL CMD AMCRDA 5001 EISENHOWER AVE ALEXANDRIA VA 22333-0001
1	INST FOR ADVNCD TCHNLGY THE UNIV OF TEXAS AT AUSTIN PO BOX 202797 AUSTIN TX 78720-2797
1	DARPA B KASPAR 3701 N FAIRFAX DR ARLINGTON VA 22203-1714
1	US MILITARY ACADEMY MATH SCI CTR OF EXCELLENCE MADN MATH MAJ HUBER THAYER HALL WEST POINT NY 10996-1786
1	DIRECTOR US ARMY RESEARCH LAB AMSRL D D R SMITH 2800 POWDER MILL RD ADELPHI MD 20783-1197

NO. OF COPIES	ORGANIZATION
1	DIRECTOR US ARMY RESEARCH LAB AMSRL DD 2800 POWDER MILL RD ADELPHI MD 20783-1197
1	DIRECTOR US ARMY RESEARCH LAB AMSRL CI AI R (RECORDS MGMT) 2800 POWDER MILL RD ADELPHI MD 20783-1145
3	DIRECTOR US ARMY RESEARCH LAB AMSRL CI LL 2800 POWDER MILL RD ADELPHI MD 20783-1145
1	DIRECTOR US ARMY RESEARCH LAB AMSRL CI AP 2800 POWDER MILL RD ADELPHI MD 20783-1197
	ABERDEEN PROVING GROUND
4	DIR USARL AMSRL CI LP (BLDG 305)

NO. OF COPIES	ORGANIZATION
1	CDR US ARMY ARDEC G FLEMING PICATINNY ARSENAL NJ 07806-5000
2	CDR US ARMY ARDEC AMSTA AR FSA E E BAKER D KAPOOR PICATTINY ARSENAL NJ 07806-5000
2	SOUTHWEST RSRCH INST C ANDERSON J LANKFORD PO DRAWER 28510 SAN ANTONIO TX 78228-0510
1	DIRECTOR LOS ALAMOS NATIONAL LAB MS B296 G T GRAY PO BOX 1663 LOS ALAMOS NM 87545
1	US AIR FORCE WRIGHT LAB TECH LIB J FOSTER ARMAMENT DIV 101 EGLIN AVE STE 239 EGLIN AFB FL 32542
1	LOS ALAMOS NATIONAL LAB D RABERN GROUP MEE 13 MSJ576 LOS ALAMOS NM 87545
1	LOS ALAMOS NATIONAL LAB TECH LIB PO BOX 1663 LOS ALAMOS NM 87545
1	JOHNS HOPKINS UNIV DEPT MECH ENGINEERING K RAMESH CHARLES AND 33 ST BALTIMORE MD 21218

NO. OF COPIES	ORGANIZATION
5	CDR US ARMY TACOM AMSTA TR S T FURMANIAK S GOODMAN D TEMPLETON C BISHNOI AMSTA TR E MATL B ROOPCHAND WARREN MI 48397-5000
1	PENN STATE UNIV COLLEGE OF ENGINEERING R GERMAN UNIVERSITY PARK PA 16802-6809
1	CALTECH G RAVICHANDRAN MS 105-50 1201 E CALIFORNIA BLVD PASADENA CA 91125
1	INST OF ADVANCE TECH UNIV OF TX AUSTIN S J BLESS 4030 2 W BRAKER LN AUSTIN TX 78759
1	CDR US ARMY RSRCH OFFICE A RAJENDRAN PO BOX 12211 RESEARCH TRIANGLE PARK NC 27709-2211
1	VIRGINIA POLYTECHNIC INST COLLEGE OF ENG R BATRA BLACKSBURG VA 24061-0219
1	DIR LLNL D LASILA L 170 LIVERMORE CA 94550

NO. OF
COPIES ORGANIZATION

ABERDEEN PROVING GROUND

54 DIR USARL
AMSRL WM TD
B BURNS
A M DIETRICH
D DANDEKAR (15 CPS)
D GROVE
T HADUCH
J M BOTELER
S SCHOENFELD
E RAPACKI
N RUPERT
K FRANK
M RAFTENBERG
T WRIGHT
P KINGMAN
S SEGLETES
T WEERASOORIYA
AMSRL WM TC
T BJERKE
E KENNEDY
R MUDD
W WALTERS
L MAGNESS
R COATES
B SORENSON
D SCHEFFLER
K KIMSEY
AMSRL WM TA
W GILLICH
W BRUCHEY
M BURKINS
J RUNYEON
W A GOOCH
B BARTKOWSKI
M NORMANDIA
AMSRL WM MC
R ADLER
M STAKER
E CHIN
AMSRL WM MD
W DEROSSET
R DOWDIN
K CHO
AMSRL WM MB
B FINK
C HOPPEL
G GASONAS

INTENTIONALLY LEFT BLANK.

REPORT DOCUMENTATION PAGE

Form Approved
OMB No. 0704-0188

1. AGENCY USE ONLY *(Leave blank)*	2. REPORT DATE	3. REPORT TYPE AND DATES COVERED
	February 2001	Final, Oct 1999 - Sep 2000

4. TITLE AND SUBTITLE
Deformation of a Low-Cost Ti-6A1-4V Armor Alloy Under Shock Loading

5. FUNDING NUMBERS
0601102AH42

6. AUTHOR(S)
Stephen V. Spletzer and Dattatraya P. Dandekar

7. PERFORMING ORGANIZATION NAME(S) AND ADDRESS(ES)
U.S. Army Research Laboratory
ATTN: AMSRL-WM-TD
Aberdeen Proving Ground, MD 21005-5066

8. PERFORMING ORGANIZATION REPORT NUMBER
ARL-TR-2386

9. SPONSORING/MONITORING AGENCY NAMES(S) AND ADDRESS(ES)

10.SPONSORING/MONITORING AGENCY REPORT NUMBER

11. SUPPLEMENTARY NOTES

12a. DISTRIBUTION/AVAILABILITY STATEMENT
Approved for public release; distribution is unlimited.

12b. DISTRIBUTION CODE

13. ABSTRACT ***(Maximum 200 words)***

The shock behavior of a new, low-cost Ti-6Al-4V alloy has been characterized up to stress levels of 20 GPa. Examination of the particle velocity histories obtained from specimens of the alloy during 11 plate-on-plate impact/planar shock wave experiments indicates that the alloy deforms in an elastic-plastic manner. The magnitude of the Hugoniot Elastic Limit (HEL) lies between 2.0 and 3.0 GPa and appears to be dependent upon material thickness. Plastic shock velocity increases with increasing stress and varies from 5.20 to 5.53 mm/μs. Reshock experiments indicate material work hardening. Shear strength sustained during plastic deformation also tends to increase with stress and ranges from 0.5 to 0.9 GPa. Spall strength thresholds tend to vary with changes in pulse width and ranges from 3.1 to 4.2 GPa.

14. SUBJECT TERMS	15. NUMBER OF PAGES
low-cost Ti-6A1-4V, shock loading, deformation	53
	16. PRICE CODE

17. SECURITY CLASSIFICATION OF REPORT	18. SECURITY CLASSIFICATION OF THIS PAGE	19. SECURITY CLASSIFICATION OF ABSTRACT	20. LIMITATION OF ABSTRACT
UNCLASSIFIED	UNCLASSIFIED	UNCLASSIFIED	UL

INTENTIONALLY LEFT BLANK.

USER EVALUATION SHEET/CHANGE OF ADDRESS

This Laboratory undertakes a continuing effort to improve the quality of the reports it publishes. Your comments/answers to the items/questions below will aid us in our efforts.

1. ARL Report Number/Author ARL-TR-2386 (Spletzer) Date of Report February 2001

2. Date Report Received _____

3. Does this report satisfy a need? (Comment on purpose, related project, or other area of interest for which the report will be used.) _____

4. Specifically, how is the report being used? (Information source, design data, procedure, source of ideas, etc.) _____

5. Has the information in this report led to any quantitative savings as far as man-hours or dollars saved, operating costs avoided, or efficiencies achieved, etc? If so, please elaborate. _____

6. General Comments. What do you think should be changed to improve future reports? (Indicate changes to organization, technical content, format, etc.) _____

CURRENT ADDRESS

_____
Organization

_____
Name E-mail Name

_____
Street or P.O. Box No.

_____
City, State, Zip Code

7. If indicating a Change of Address or Address Correction, please provide the Current or Correct address above and the Old or Incorrect address below.

OLD ADDRESS

_____
Organization

_____
Name

_____
Street or P.O. Box No.

_____
City, State, Zip Code

(Remove this sheet, fold as indicated, tape closed, and mail.)
(DO NOT STAPLE)